ORIGINAL ARTICLE

Surfactant-supported organoclay for removal of anionic food dyes in batch and column modes: adsorption characteristics and mechanism study

Aya G. Mostafa[1] · Ahmed I. Abd El-Hamid[2] · Magda A. Akl[1]

Abstract

This study aimed to create CTAB-modified bentonite organoclay (Bt@CTAB) by mixing the naturally occurring mineral bentonite (Bt) with the cationic surfactant cetyltrimethylammonium bromide (CTAB). Elemental analysis, N_2 adsorption–desorption isotherm, scanning electron microscopy (SEM), FTIR spectroscopy, XRD, and thermogravimetric (TGA) analysis have been employed to analyze both the unmodified Bt and the Bt@CTAB organoclay. The dye sorption onto Bt@CTAB organoclay was investigated in the batch and column modes using aqueous solutions of anionic food dyes, viz., Sunset yellow FCF (E110), Azorubine (E122), and Ponceau 4R (E124) (individually or in a mixture). Experimental variables affecting the adsorption process, such as initial dye concentration, contact time, temperature, pH, and adsorbent dose, are evaluated. From the kinetic investigations, the adsorption of E110, E122, and E124 dyes well matched the pseudo-second-order kinetic model. E110 and E122 dyes adsorption onto Bt@CTAB attained equilibrium in 120 min while attained in 240 min for E124. The investigated food dyes were expected to achieve maximum adsorption efficiencies at concentration of 100 ppm of (E110 and E124) and 150 ppm of (E124), an adsorbent dosage of 0.4 gL^{-1}, and an initial pH 5. In addition, Langmuir model best fits the sorption isotherm data, with the maximum adsorption capacity at 303 K being 238 mg/g, 248.75 mg/g, and 358.25 mg/g for E110, E122, and E124, respectively. The Bt@CTAB organoclay can be regenerated up to the 4th cycle successfully. The thermodynamic studies revealed the spontaneous and exothermic nature of the adsorption of these anionic dyes onto Bt@CTAB organoclay. The prepared cationic Bt@CTAB organoclay was successfully applied for the removal of E110, E122, and E124 from real water samples, synthetic effluents, and colored soft drinks with a recovery (R%) higher than 95%. The plausible adsorption mechanism of E110, E122, and E124 onto Bt@CTAB organoclay is proposed to be due to electrostatic interaction and hydrogen bond formation. Finally, the present study shows that Bt@CTAB organoclay may be employed efficiently and effectively to remove anionic food dyes from a wide range of real water and colored soft drinks.

Keywords Bentonite · Organoclay · Food dyes · Anionic dyes · E110 · E122 · E124 · Adsorption

Introduction

Globally, we not only need to deal with water deficiency but also the problem of water pollution from hazardous toxins (El-Kowrany et al. 2016; Karri et al. 2021; WHO 2017).

✉ Magda A. Akl
magdaakl@yahoo.com

1 Chemistry Department, Faculty of Science, Mansoura University, Mansoura 35516, Egypt

2 Advanced Technology and New Materials Research Institute, City of Scientific Research and Technological Applications (SRTA-City), P. O. Box 21934, Alexandria, Egypt

Sewage discharge has increased as well due to fast industrial growth. Hazardous aromatic compounds, metals, and dyes are only some of the organic and inorganic components found in this wastewater (Saleem et al. 2019; Srivastav and Ranjan 2020; Muhammad et al. 2021; Zamora-Ledezma et al. 2021). Some dyes and pigments have been labeled as hazardous compounds due to their potential toxicity to human health. They are harmful, consume a long time to decompose in landfills or water treatment plants, and impair water transparency (Berradi et al. 2019; Moore 1999). As there is enough evidence, prolonged exposure to dyes and their compounds may cause cancer and other serious health problems. Furthermore, the disruption of the photosynthetic cycle induced by textile effluent in waterways disrupts the

delicate balance of aquatic life and the food chain (Affat 2021).

Azo dyes are considered the most widely utilized dyes in several industries (food, textiles, cosmetics, paper, leather, pharmaceutical, rubber, pesticide, varnish, petrochemical, electroplating, etc.) (Balayeva et al. 2021; Hamada and Jabal 2022; Salahuddin et al. 2018; Toutounchi et al. 2021). Synthetic food dyes such as Ponceau 4R ($C_{20}H_{11}N_2Na_3O_{10}S_3$, E124), Sunset yellow ($C_{16}H_{10}N_2Na_2O_7S_2$, E110), and Azorubine ($C_{20}H_{12}N_2Na_2O_7S_2$, E122) are used in the food industry due to their advantages as they are stable, available, low-cost, manufactured simply, and require short time. These dyes are nonbiodegradable as they have physicochemical, thermal, and optical stability. Their stability is because of their chemical structure as they have symmetrical aromatic groups (Laptev et al. 2021; Leulescu et al. 2021; Lima et al. 2019; Micheletti et al. 2020). Moreover, they have bad impacts on human health including harmful and carcinogenic effects as they may cause cancer to many organs such as the bladder, liver, and kidney. In addition, they may result in mood swings and hyperactivity in adults and children. So, their elimination is essential in order to overcome their adverse effects (Abd-Ellatif et al. 2022; Alham et al. 2022).

Methodologies (Ashraf et al. 2021) including photocatalytic degradation (Akl et al. 2022b; Waghchaure et al. 2022), electrochemical oxidation (Shi et al. 2020), solvent extraction (Prusty and Pradhan 2021), membrane filtration (Hube et al. 2020), Fenton (Rafaqat et al. 2022), and adsorption have proven efficient in cleaning up industrial wastewaters before they are released into the environment (Mostafa et al. 2021; Akl et al. 2022a; El Ouachtak et al. 2018; Yaghmaeiyan et al. 2022; Zou et al. 2019). Adsorption has recently been shown to be favored over other methods owing to its simple operation, low cost, adaptability in design, and insensitivity to harmful pollutants (Wang et al. 2009). The selection of adsorbents is crucial to the process's technical applicability and economic viability (Iwuozor et al. 2021; Saleem et al. 2019). Wastewater decontamination may make use of nontraditional adsorbents, including natural materials, agricultural industry wastes, carbon materials, and biosorbents. Activated carbon has been the most popular adsorbent due to its high capacity for absorbing organic dyestuffs (Husien et al. 2022).

Clays are widely used adsorbents as they are cheap, effective, and available. Moreover, they have high cation exchange capacity and high swelling capability. Bentonite is primarily montmorillonite-based clay and consists of an alumina layer between two silicon–oxygen tetrahedron layers. However, there are two mean reasons for bentonite's low adsorption efficiency: the deprotonation of bentonite hydroxyl groups at high pH and the existence of negative charges on its surface. Moreover, some studies proved that bentonite activity is enhanced by modifying its surface. Silicone cationic surfactants provide siloxane groups with hydrophobicity properties, have climate resistance, reduced surface tension, and organic matter content increases. These new characteristics enhanced the adsorption efficiency (Alexander et al. 2019; Rizzi et al. 2020; Tamjidi et al. 2021; Tebeje et al. 2022). Cetyltrimethylammonium bromide (CTAB) is a cationic surfactant that exhibits good surface activity, antibacterial activity, and stability in both alkaline and highly acidic mediums. The modification of bentonite with the CTAB surfactant results in improving its intralayer structure surface electrical properties leading to bentonite adsorption efficiency enhancement for anionic species. The effectiveness of Bt@CTAB in eliminating anionic dyes has been shown in a variety of research studies (Huang et al. 2017; Y. Wang et al. 2021).

The objectives of the present study can be presented in the following points:

1. Design and characterization of native bentonite and cationic Bt@CTAB organoclay using nitrogen (N_2), elemental analysis, SEM, FTIR, XRD, and TGA and performances.
2. Experimental investigation (in batch and column modes) of anionic food dyes E110, E122, and E124 adsorption utilizing Bt@ CTAB organoclay in aqueous solutions.
3. Studying the adsorption of E110, E122, and E124 anionic food dyes in a binary system.
4. Investigating the different experimental parameters affecting the adsorption process of E110, E122, and E124 anionic dyes onto Bt@CTAB, e.g., adsorbent dosage, pH, initial E110, E122, and E124 concentrations, and ionic strength.
5. Conducting adsorption isotherm and kinetic experiments to understand the adsorption mechanism and highest adsorption ability of Bt@CTAB.
6. Application of the prepared Bt@CTAB organoclay on real water and soft drinks samples.
7. Elucidation of adsorption mechanism of E110, E122, and E124 anionic food dyes onto Bt@CTAB organoclay.

Experimental

Materials

In this work, the used Bt was collected from Egypt and was crushed and sieved using a 200-mesh screen that permits the passage of particles with a size < 74 microns. The chemical composition of the bentonite (Bt) is present in Table S1. The used chemicals are NaOH, EDTA, CH_3COONa, HCl, NaCl, Na_2CO_3, ethanol, Sunset yellow FCF (E110), Azorubine (E122), Ponceau 4R (E124) anionic food dyes, and cetyltrimethylammonium bromide (CTAB) surfactant

with Mwt 364.4 g/mol. All these chemicals were obtained from Sigma-Aldrich and were of analytical grade.

Equipment

Utilizing a Perkin-Elmer 550 spectrophotometer for determining anionic dyes (E110, E122, and E124) and binary systems (E110-E122, E110-E124, E122-E124, and E110-E122-E124) concentration over a range of 200–900 nm using quartz cells, the λ_{max} is of E110 (486 nm), E122 (518 nm), E124 (508 nm), E110-E122 (508 nm), E110-E124 (500 nm), E122-E124 (518 nm), and E110-E122-E124 (512 nm).

The FTIR spectra of native Bt, Bt@CTAB, Bt@CTAB-E110, Bt@CTAB-E122, and Bt@CTAB-E124 were investigated by (Perkin-Bhaskar-Elmer Co., USA). Clay samples were grounded and mixed with KBr and then pressed in pellets form. JSM-6510LV model was utilized for the investigation of surface morphology samples. Estimation of the CNH composition of Bt and Bt@CTAB organoclay was obtained by a Costech ECS-4010 elemental analyzer. The specific surface area of the Bt and Bt@CTAB materials was obtained using the Brunauer–Emmet–Teller (BET) analysis (Size Analyzer (QUANTACHROME–NOVA 2000 Series)). The thermal stability of Bt and Bt@CTAB materials was examined by thermogravimetric analysis (Perkin Elmer TGA 4000) at a heating rate of 15 °C/min from 30 to 800 °C. X-ray diffraction (XRD) patterns of the Bt and Bt@CTAB samples were obtained by a PANalytical X'Pert PRO diffractometer over the 2-theta (2θ) range from 4° to 70°. The pH$_{PZC}$ of Bt@CTAB was determined as follows: 0.1 g of the Bt@CTAB clay adsorbent was added to a 25 ml of pH-adjusted NaCl (0.01 M) solution that varied from 2 to 12, and the mixtures were allowed to shake at the equilibrated shaker for 48 h. 0.1 M of HCl and 0.1 M of NaOH were utilized for NaCl pH adjustment. After shaking, the final pH was recorded and ΔpH was measured as in the following Eq (ΔpH = pHi-pHf) and was plotted against the initial pH (pHi). The pH$_{PZC}$ value is the cross point where the curve ΔpH vs pHi crosses the line ΔpH = 0 (Ouachtak et al. 2021).

Preparation of Bt@CTAB adsorbent

Bt@CTAB organoclay was prepared according to previously published studies (Monteiro et al. 2018; Youssef and Al-Awadhi 2013). The first step in organo-bentonite (Bt@CTAB) synthesis was the dispersion of 25 g of the native Bt clay in dist.H$_2$O for 60 min. Then the next step was to gradually add to the suspended Bt an amount corresponding to 1 mmol/g CEC (cation exchange capacity). The Bt and CTAB mixture was allowed to stir at 60°C for 6 h. Then the mixture was centrifuged with a speed of 3000 rpm and

washed many times by the dist.H$_2$O in order to remove any excess of the CTAB surfactant. The last step was to dry the produced Bt@CTAB powder for 24 h in an oven at 70 °C.

Adsorption and regeneration procedures

Batch tests

The maximum absorption spectra (λ_{max}) of E110, E122, E124, and different mixtures (E110-E112, E110-E122, E122-E124, and E110-E122-E124) were obtained through the scanning of their solutions in the range of (190–1100 nm). E110 (486 nm), E122 (518 nm), and E124 (508 nm) dyes adsorption studies were performed at concentrations ranging from 50 to 400 mg/L. For dyes binary systems adsorption experiments, the dyes were mixed by a ratio of 1:1 for (E110-E112, E110-E122, and E122-E124) and 1:1:1 for the E110-E122-E124 binary system. The adsorption experiments of the investigated food dyes were performed in 125-ml stoppered bottles that contained 25 ml of anionic dye solution and adsorbent Bt@CTAB dose (0.01 g). Then, these bottles were shaken at 150 rpm on a thermostated shaker at room temperature. After the equilibrium was reached, the solutions were centrifuged at 3000 rpm. The supernatant solution that includes the remains of the investigated anionic dyes was measured at the specific λ_{max} of each dye. Samples after adsorption were scanned regularly between 200 and 900 nm at different time intervals to obtain the lambda maximum. Various parameters were studied such as contact time (15–300 min), temperature (25–45 °C), Bt@CTAB adsorbent dose (0.005–0.03 g), pH (from 2 to 11), ionic strength, and initial concentration of dye (25–400 mg/l). The anionic dye removal percentage (R, (%)) and adsorption capacity (q_e) of dyes were calculated as per Eqs. (1) and (2), respectively (Akl et al. 2022a).

$$R\% = \frac{C_i - C_f}{C_i} \times 100 \tag{1}$$

$$q_e = \frac{(C_i - C_f) \times V}{wt} \times 100 \tag{2}$$

where C_i (ppm) and C_f (ppm) are the initial anionic dyes concentration and equilibrium anionic dyes concentration, respectively. V (L) is the volume of investigated dye, and wt (g) is the Bt@CTAB dose.

Desorption and regeneration investigation

After the adsorption of E110, E122, and E124 food dyes by Bt@CTAB clay, desorption of the investigated dyes was examined by different eluents including ethanol, NaOH (0.2 mol/L), and sod. bicarbonate (0.2 mol/L), CH$_3$COONa (0.1 mol/L), and HCl

(0.2 mol/L). The regeneration of Bt@CTAB organoclay was examined through five repeated cycles of adsorption–desorption by the batch method. 0.01 g of Bt@CTAB was shaken with 25 ml of (100 ppm for E110 and E122) and 150 ppm for E124) for 120 min for E124 and 240 min for (E110 and E124); then, adsorbent was filtered and then it was eluted with absolute ethanol and these procedures were repeated for another 4 cycles. The investigated food dyes desorption (D, %) Bt@CTAB organoclay was calculated from Eq. (3) (Akl et al. 2022b)

$$
\begin{aligned}
&\text{De} - \text{sorption\%} \\
&= \frac{\text{amount dseorbed to the solution(mg/l)}}{\text{amount adsorbed on NAgDFF(mg/l)}} \times 100
\end{aligned}
\tag{3}
$$

Column investigations

The use of Bt@CTAB organoclay as a filter was investigated through the column experiments studying. A mass of Bt@CTAB organoclay was pressed and put in the column bottom. The investigation of the optimum parameters is column diameter (0.7 and 0.9 cm), organoclay weight which varied from 0.0025 g to 0.05 g, flow rates of anionic dyes (slow 0.16 ml/min) and fast (0.42 ml/min) using 100 ppm E110 and E122 and 150 ppm of E124 at optimum pH that was obtained from the batch investigations. The concentrations E110, E122, and E124 after passage through the column were determined spectrophotometrically at specific λ_{max} of each dye. The removal percentage ($R\%$) was determined as in Eq. (1) (Akl et al. 2022a).

Kinetics, isothermal, and thermodynamics

Effect of initial concentration and isothermal investigation

The isothermal investigations for E110, E122, and E124 adsorption were performed by placing 0.01 g of Bt@CTAB organo-clay adsorbent in a series of bottles containing E110/E122/E124 dye solution. The initial dye concentration was in the range of (50–400 mg/L). These bottles were placed in a thermostated shaker with a shaking speed of 150 rpm at 25 °C for 120 min for E124 and 240 min for E110 and E122 at pH 5. Dubinin–Radushkevich (D-R), Langmuir, and Freundlich's isothermal models were applied in the linear form, and the parameters were calculated as shown in Eqs. (4), (5), and (6), respectively. Langmuir separation factor (R_L) presented in Eq. (7) is an essential parameter. It is used in adsorbent-sorbate affinity prediction. The indications of values of R_L are illustrated as follows: If it is greater than 1.0, this means the unsuitability of the investigated adsorbent, while if it occurred in the range from 0 to 1, it means the suitability of the utilized adsorbent (Akl et al. 2022b).

$$
\ln q_e = \ln q_m - K_{DR}\varepsilon^2
\tag{4}
$$

$$
\frac{C_e}{q_e} = \frac{1}{k_L q_m} + \frac{C_e}{q_m}
\tag{5}
$$

$$
\ln q_e = \ln K_F + \frac{1}{n}\ln C_e
\tag{6}
$$

$$
R_L = \frac{1}{1 + K_L C_o}
\tag{7}
$$

As C_e (mg/L) is the anionic dyes (E110, E122, and E124) concentration at equilibrium, q_e (mg/g) is the dye capacity at equilibrium, q_m (mg/g) is adsorption maximum amount, $1/n$ is the heterogeneity factor, while K_L (L/mg), K_F (mg/g), and K_{DR} are Langmuir, Freundlich constants, the Dubinin–Radushkevich constants, respectively. ε is the adsorption potential and is given by Eq. (8).

$$
\varepsilon = RT\ln\left(+\frac{1}{C_e}\right)
\tag{8}
$$

where R (8.314 J/mol K) is the gas constant, and T is the temperature (K) at which adsorption occurred.

Effect of contact time and kinetic studies

For estimation of the adsorption rate-limiting step, kinetic investigations were carried out using two kinetic models: pseudo-1st order and pseudo-2nd order which are presented in Eqs. 9 and 10, respectively [44]. The investigations were performed at the optimum pH for each dye using 25 ml (100 ppm of (E110 and E122), 150 ppm of (E124)) and 0.01 g of the Bt@CTAB adsorbent which were allowed to shake with different contact times varied from 15 to 300 min in a thermostated shaker at the room temperature with constant speed 150 rpm.

$$
\frac{1}{q_t} = \frac{K_1}{q_e t} + \frac{1}{q_e}
\tag{9}
$$

$$
\frac{t}{q_t} = \frac{1}{K_2 q_e^2} + \frac{t}{q_e}
\tag{10}
$$

The adsorption efficiency for investigated food dyes at equilibrium and at a certain time t (min) is expressed as q_e (mg/g) and q_t (mg/g), respectively. As well as K_1 and K_2 are constants for pseudo-1st order and pseudo-2nd order, respectively.

Effect of temperature and thermodynamic studies

A series of 125-ml stoppered bottles containing 25 ml of anionic dyes' solution (100 mg/L for (E110 and E122) and 150 mg/L for E124) and 0.01 g of Bt@CTAB at different

temperatures (25–45) °C and optimum pH 5 were shaken for 240 min for (E110 and E122) and 120 min for E124 in an equilibrated shaker at constant speed 150 rpm. The residual (E110, E112, and E124) dye concentration was determined after adsorption and filtration.

Thermodynamic parameters (adsorption enthalpy ($\Delta H°$), adsorption free energy ($\Delta G°$), and adsorption entropy ($\Delta S°$)) are expressed in Eqs. (11) and (12) and were calculated as follows; $\Delta S°$ and $\Delta H°$ were calculated from Eq. (12) intercept that equals $\Delta S°/R$ and slope that equals $-\Delta H°/R$ of Ln K_c vs. $1/T$. A gas constant expressed as (R) equals 8.314 J/mol K (Saleh et al. 2021).

$$\Delta G° = -RT \ln K_c \tag{11}$$

$$\ln K_c = \frac{\Delta S°}{R} - \frac{\Delta H°}{RT} \tag{12}$$

Analysis of real samples

Analysis of real water samples

The spiking of the (100 ppm for (E110 and E122) and 150 ppm for (E124)) into the real water samples (seawater, wastewater, and tap water) was carried out. Prior to the spiking of the dyes, the real water samples were digested by adding 0.5 g of $K_2S_2O_8$, and 5 ml H_2SO_4 98% (w/w) to 1000 ml of water sample and heated for 120 min at 90 °C for complete digestion of presented organic materials. After cooling to room temperature, 0.01 g of Bt@CTAB-modified clay was added to the prepared samples and the pH value

Table 1 The textural properties of the investigated bentonite and Bt@CTAB as determined from nitrogen adsorption isotherms

Adsorbent	Surface area SBET (m²/g)	BET-C constant	Pore volume VT (ml/g)	Aver. pore diameter (nm)
Bt	32.17	75.29	0.029	1.8
Bt@CTAB	18.41	37.13	0.015	1.66

Table 2 Elemental analysis of Bt and Bt@CTAB

Sample	C (%)	H (%)	N (%)
Bt	1.367	2.08	0
Bt@CTAB	11.95	3.095	0.52

was adjusted to 5 with continuous shaking for 120 min for E124 and 240 min for (E110 and E122). The solutions were centrifuged and again another 0.01 g of Bt@CTAB-modified clay was added to the supernatant to ensure the complete separation of analytes. The remaining E110/E122/E124 was determined using Unicam UV 2100 UV–Visible spectrometer at appropriate wavelengths.

Analysis of colored soft drinks and industrial food samples

Bt@CTAB organoclay was applied for the removal of E110 and E122 from degassed carbonized drinks, candy, and jelly. Carbonized drinks (an orange drink that contains E110 dye and a pomegranate drink that contains E122) are degassed first by letting them in the air at room temperature for 2 h. Candy (watermelon taste) and jelly (strawberry and orange) were digested in acetic acid 4% and then dissolved

Fig. 1 Digital photographs of **a** Bt, **b** Bt@CTAB, **c** Bt@CTAB-E122, **d** Bt@CTAB-E124, **e** Bt@CTAB-E110
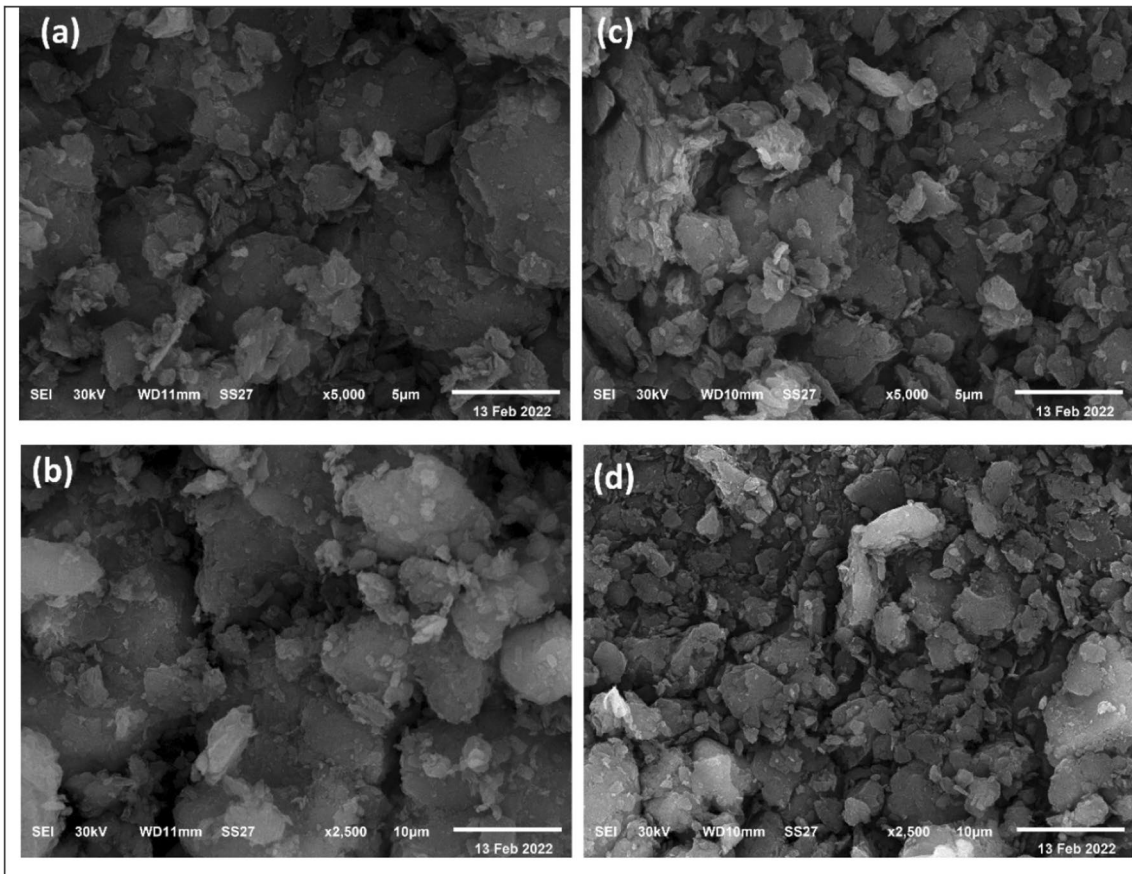
Fig. 2 a, b Native Bt and **c**, **d** Bt@CTAB SEM images

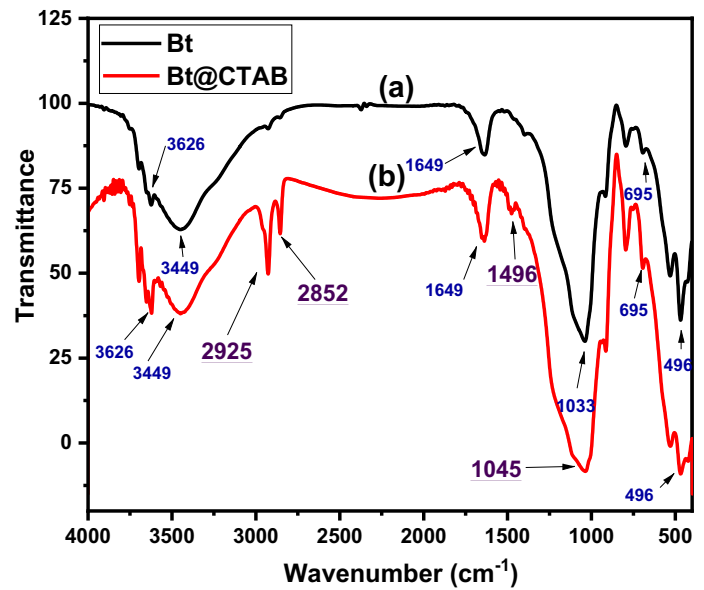**Fig. 3** IR spectra of **a** Bt and **b** Bt@CTAB

Fig. 4 IR spectra of **a** Bt@CTAB, **b** Bt@CTAB-E110, **c** Bt@CTAB-E122, and **d** Bt@CTAB-E124
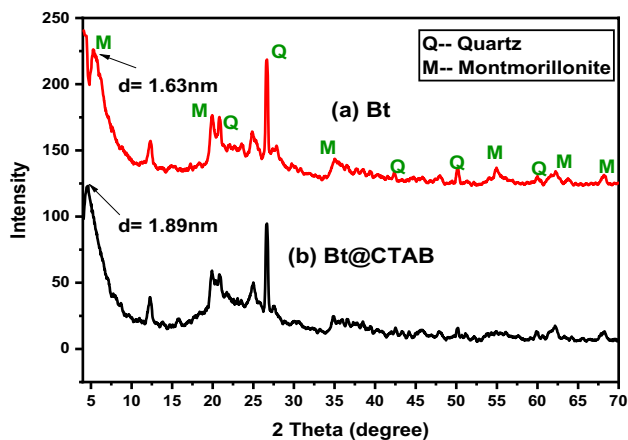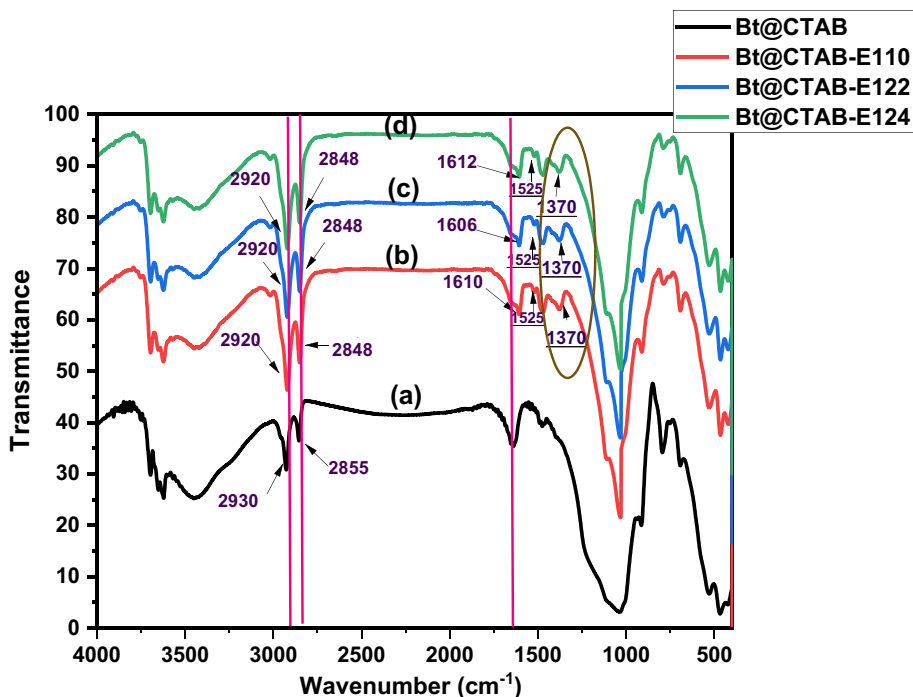

Fig. 5 XRD patterns of **a** Bt and **b** Bt@CTAB

in dist. H_2O. Bt@CTAB (0.01 g) was added to the prepared samples, and the pH of the samples was adjusted to 5 with continuous shaking for 120 min for E124 and 240 min for (E110 and E122). The dye remaining was determined using Unicam UV 2100 UV–Visible spectrometer at appropriate wavelengths.

Results and discussion

Optical images

Figure 1 (a-e) represents the Bt, Bt@CTAB, Bt@CTAB-E122, Bt@CTAB-E124, and Bt@CTAB-E110 optical images, respectively. The difference in materials' color and shape is very noticeable as the color of samples changed after the reaction with CTAB from faint yellow (Fig. 1a) to off-white color (Fig. 1b). This change of color is an evidence of the modification. The change in the clay material's color before (E110, E122, and E124) adsorption and after adsorption was taken as an evidence of dye adsorption on the clay surface as the color changed from off-white (Fig. 1b) of Bt@CTAB to bright orange in the case of E110, reddish pink in case of E122, and red in case of E124 (Fig. 1c-e). Figure S1 (a-f) represents the (E110, E122, and E124) before and after adsorption using the Bt@CTAB clay through batch experiments at the investigated ideal conditions.

Characterization

N$_2$ adsorption desorption isotherm

The adsorption isotherms of Bt and Bt@CTAB were obtained with Brunauer–Emmett–Teller (BET) surface area analysis. Table 1 represents surface areas of Bt and Bt@CTAB' S_{BET}, total pore volumes (V_T), and mean pore diameters. The results presented in Table 1 indicate that the modification of Bt with CTAB resulted in the reduction in surface area, the mean diameter, and total pore volume values for Bt@CTAB. The decrease of the specific surface area after chemical modification may be due to the covering of Bt pores by CTAB particles that results in the decrease in the adsorption of N_2 molecules that are used in the surface area measurement process.
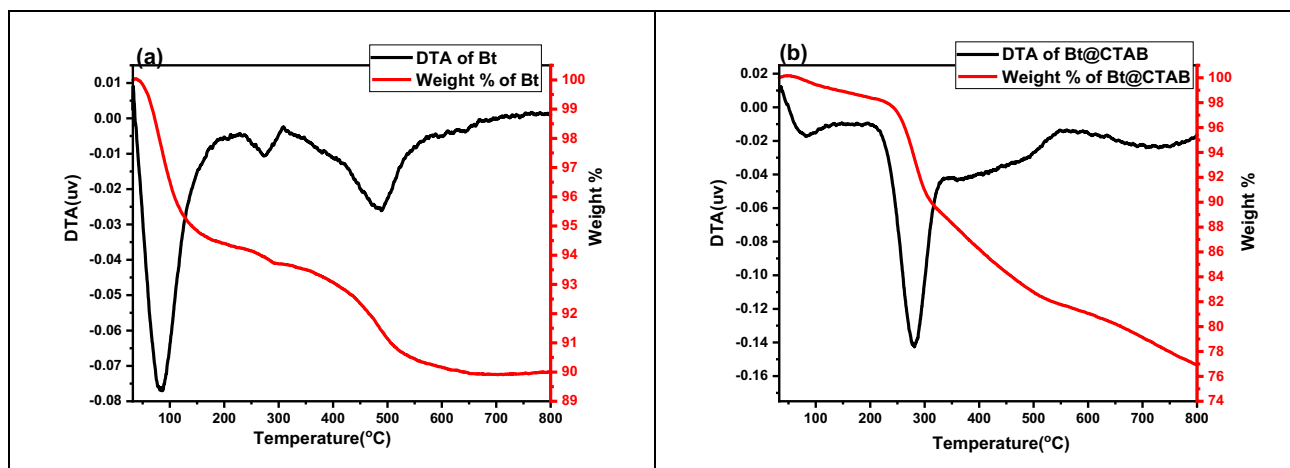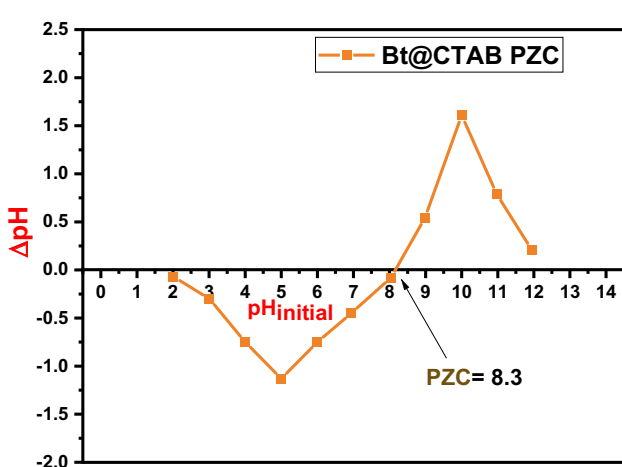
Fig. 6 TGA of **a** Bt **b** Bt@CTAB

Fig. 7 The pH$_{pcz}$ value of Bt@CTAB

Fig. 8 pH effect on E110, E122, and E124 adsorption efficiency onto Bt@CTAB of these conditions (temp.: (25 °C), dose: 0.01 g., conc.: 100 mg/L for E110 & E122 and 150 mg/L for E124, volume: 25 mL)

Elemental analysis

The CHN analysis was evaluated for Bt and Bt@CTAB materials for proving the formation of Bt@CTAB. The results presented in Table 2 show the existence of N in the Bt@CTAB sample with a percentage (0.52%) and the increase of carbon atom percentage from 1.367 to 11.95% and hydrogen atom percentage from 2.08 to 3.095%. These alterations are great evidence for the Bt clay modification by CTAB.

SEM

The surface images of Bt and Bt@CTAB are shown in Fig. 2 (a, b) and (c, d), respectively. It was revealed that the modification of Bt material results in more pores, flakes,
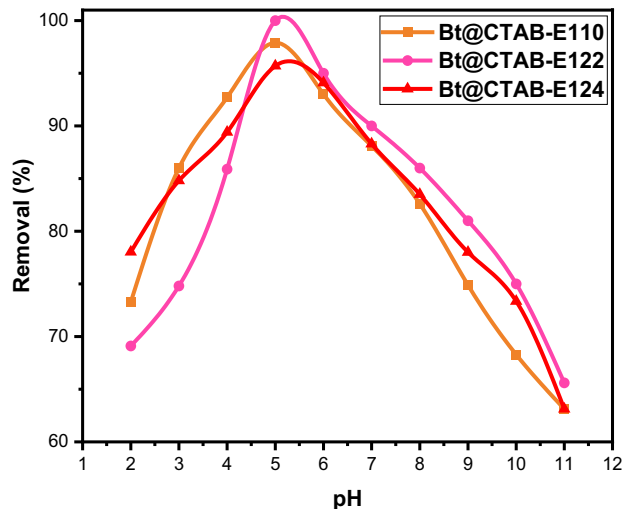
and surface roughness in the modified bentonite clay (Bt@CTAB), and these alterations may be returned to the CTAB covering for the clay surface (Ouachtak et al. 2021; Shirzad-Siboni et al. 2015).

FTIR analysis

The FTIR spectra of native Bt clay and the Bt@CTAB-modified clay, which are presented in (Fig. 3), were obtained and studied in the range of 400 cm^{-1} to 4000 cm^{-1}. Both samples (Bt and Bt@CTAB) have some identical peaks; the first peak is Si–O which appeared in the two materials as follows: at approximately 469 cm^{-1} of the (Al–O–Al) vibrational band and 1036 cm^{-1} of the (Al–O–Si) vibrational band (el Haouti
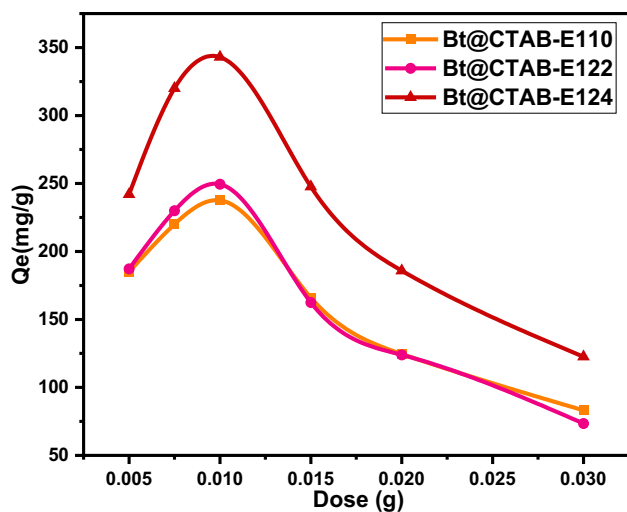
Fig. 9 Effect of dose on E110 (100 ppm), E122 (100 ppm), and E124 (150 ppm) adsorption onto Bt@CTAB at room temperature for 2 h

et al. 2019; Huang et al. 2017). The other identical peaks are those that appeared at 1470 cm^{-1} and 690 cm^{-1} which are related to Ca-Mg $(CO_3)_2$ and Al–O–Al vibrational bands, respectively (Solotchina et al. 2014). There are three new bands that appeared at 1649, 3449, and 3626 cm^{-1} corresponding to (–OH) deformation of water. The interaction of CTAB with Bt, native clay, was demonstrated by the appearance of CTAB characteristic' peaks (–CH$_3$ vibrational band and –CH$_2$ vibrational band) at 2925 and 2852 cm^{-1} (Haounati et al. 2021; Vaia et al. 1994; Y. Wang et al. 2021). Also, a bending vibration of the methylene groups can be seen at wavelength bands of 1496 cm^{-1} (Huang et al. 2017).

FTIR spectra of Bt@CTAB before (E110, E122, and E124) dyes adsorption are present in Fig. 4a, while the spectra Bt@CTAB-E110, Bt@CTAB-E122, and Bt@CTAB-E124 after adsorption are shown in Fig. 4b, c, and d, respectively. It was noticed that a new peak appeared after the adsorption of the 3 dyes (E110, E122, and E124) at about 1370 cm^{-1} which may be attributed to the SO_3^- stretching vibrational band (Bahrudin et al. 2020). There are other new peaks related to cyclic alkene (C=C) appearing at 1530 cm^{-1} for Bt@CTAB@E110 and at 1525 cm^{-1} for Bt@CTAB@E122, and at 1528 cm^{-1} for Bt@CTAB@E124. Slight shifts occurred in the peak at 1635 cm^{-1} to 1610 cm^{-1} in Bt@CTAB@E110, to 1606 cm^{-1} in Bt@CTAB@E122, and to 1612 in Bt@CTAB@E124. The peak at 3452 cm^{-1} became broader after investigating dyes adsorption which may be attributed to hydrogen bond formation. Minor shifts related to the CH$_3$ and CH$_2$ stretching vibrational bands from 2855 cm^{-1} and 2930 to 2848 cm^{-1} and to 2920 cm^{-1} after adsorption of the three dyes (Avila et al. 2021; Gamoudi and Srasra 2019; Mallakpour and Behranvand 2021).

X-Ray diffraction analysis (XRD)

XRD is an efficient analysis for bentonite intercalation presence determination as it provides an accurate interplanar spacing (d spacing) value (Zhu et al. 2023). The XRD patterns of Bt and Bt@CTAB samples are presented in Fig. 5. The major component of Na-bentonite is Na-montmorillonite (M), and the main impurity is quartz (Q). Since the impurity particles are as tiny as the particles of the clay themselves, the centrifugation methods cannot completely remove them. The d spacing of Bt is 1.63 nm which is increased to 1.89 nm after the modification process. It shows that the CTAB surfactant molecules were intercalated in the bentonite interlayer space (Liu et al. 2017; Salah et al. 2019).

Thermogravimetric analysis

The thermal stability of Bt and Bt@CTAB materials was estimated by TGA as presented in Fig. 6 It was observed three decomposition steps with a lower mass loss value (10%) for Bt, while four decomposition steps were observed with 23.1% mass loss for the Bt@CTAB. For both Bt and Bt@CTAB, the first decomposition step below 100 °C can be attributed to the desorption of the water molecules that were related to the clay interlayer cations. As the water molecules of crystallization require a temperature higher than that of the associated ones, the 8.5% weight loss at 490 °C may be returned to their desorption, while in Fig. 6b the decomposition steps between 200 and 600 °C correspond to the organic surfactant (CTAB) decomposition (Mishra et al. 2012; Moslemizadeh et al. 2016; Motawie et al. 2014).

Adsorption studies

Point of zero charge (PZC)

The pH$_{pzc}$ of Bt@CTAB was determined utilizing a previously published approach. For this purpose, 0.01 M NaCl solutions were applied and their pH was adjusted in the 2–12 range by using 0.1 M HCl or 0.1 M NaOH solution. Then, 0.1 g of the investigated material (Bt@CTAB) was added to these solutions and shaken for 48 h, and finally, the solution pH$_{final}$ was calculated. Figure 7 shows the change of pH value (pH$_{initial}$–pH$_{final}$) of Bt@CTAB as a function of the pH$_{initial}$. From these findings, the pH$_{pcz}$ value of Bt@CTAB is determined to be 8.3. This shows that at pH below 8.3, the Bt@CTAB surface is considered to have a positive charge.
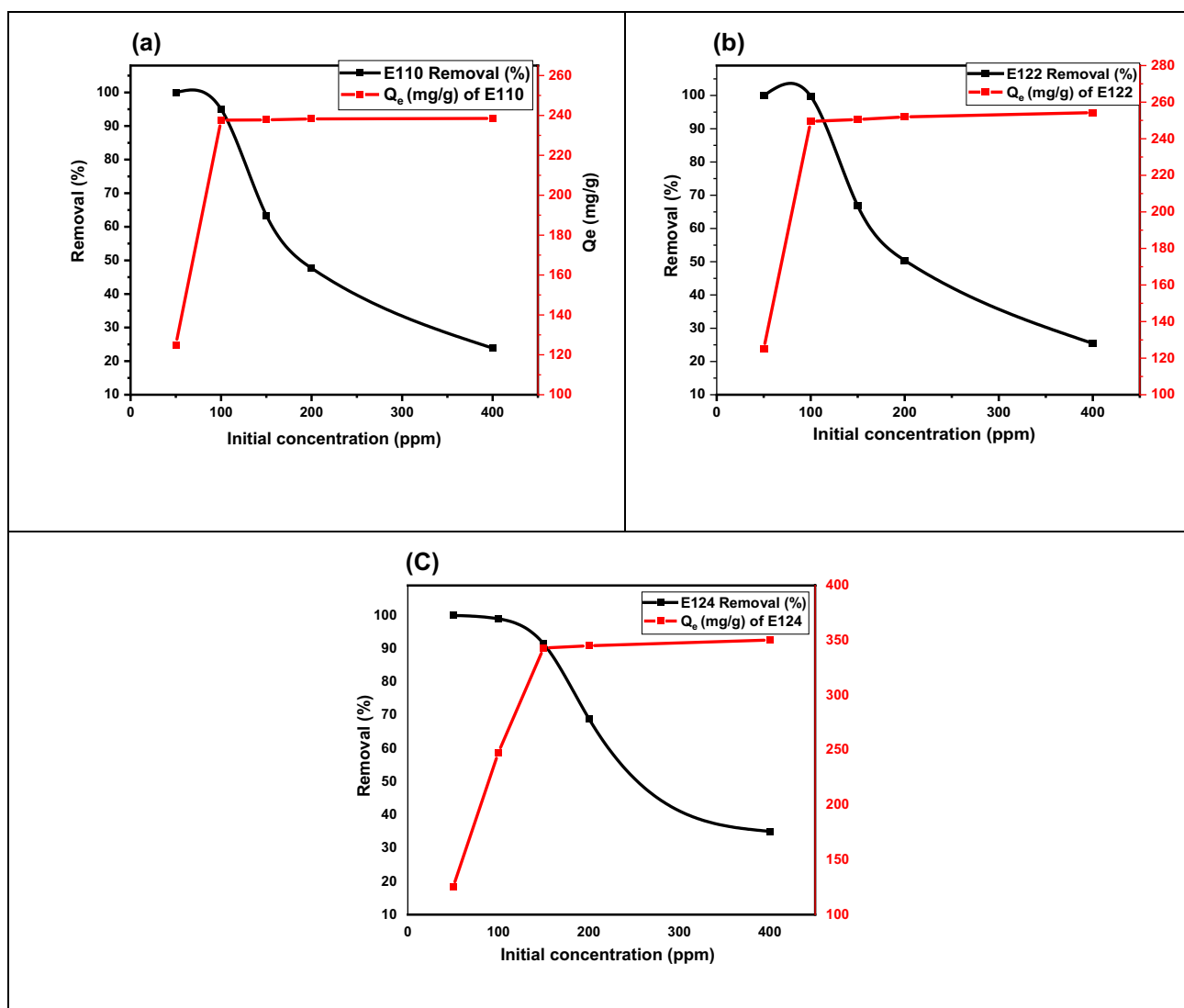
Fig. 10 a Effect of initial concentration on E110 adsorption, **b** effect of initial concentration on E122 adsorption, **c** effect of initial concentration on E124 adsorption

Effect of pH

Solid–liquid interactions are highly affected by the aqueous solution's pH through the surface functional group protonation–deprotonation, so the pH parameter is very important to be studied (Largo et al. 2020; Ouachtak et al. 2018). So, the influence of solution pH on the E110, E122, and E124 anionic species removal using Bt@CTAB was investigated in the range of 2–11. The investigation was obtained by using 25 ml of 100 ppm of E110 and E122 and 25 ml of 150 ppm of E124 and 0.01 g of Bt@CTAB at room temperature. Figure 8 illustrates that the Bt@CTAB adsorption efficiency increased from 73.28 to 97.9%, from 69.11 to 100%, and from 78.03 to 95.7% for E110, E122, and E124 adsorption, respectively, with pH increasing

from 2 to 5. Then at a pH above 5, the three investigated dyes' adsorption efficiency decreased. From the pH_{PZC} value ($+ ve < pH_{PZC}$ 8.3 $> -ve$), below pH_{PZC}, the surface of Bt@CTAB is positive allowing the adsorption of anionic dyes. That is the main reason for increasing the adsorption of E110, E122, and E124 at pH (2–5) surface (the acidic media facilitates the adsorption of the anionic dyes).

Effect of dose

The effect of the adsorbent dose was obtained by using different amounts of Bt@CTAB in 25 ml 100 ppm of E110/ E122 and 150 ppm of E124 with a shaking time of 2 h at room temperature. As shown in Fig. 9, with Bt@CTAB dose increasing from 0.005 g to 0.01 g, the capacity of
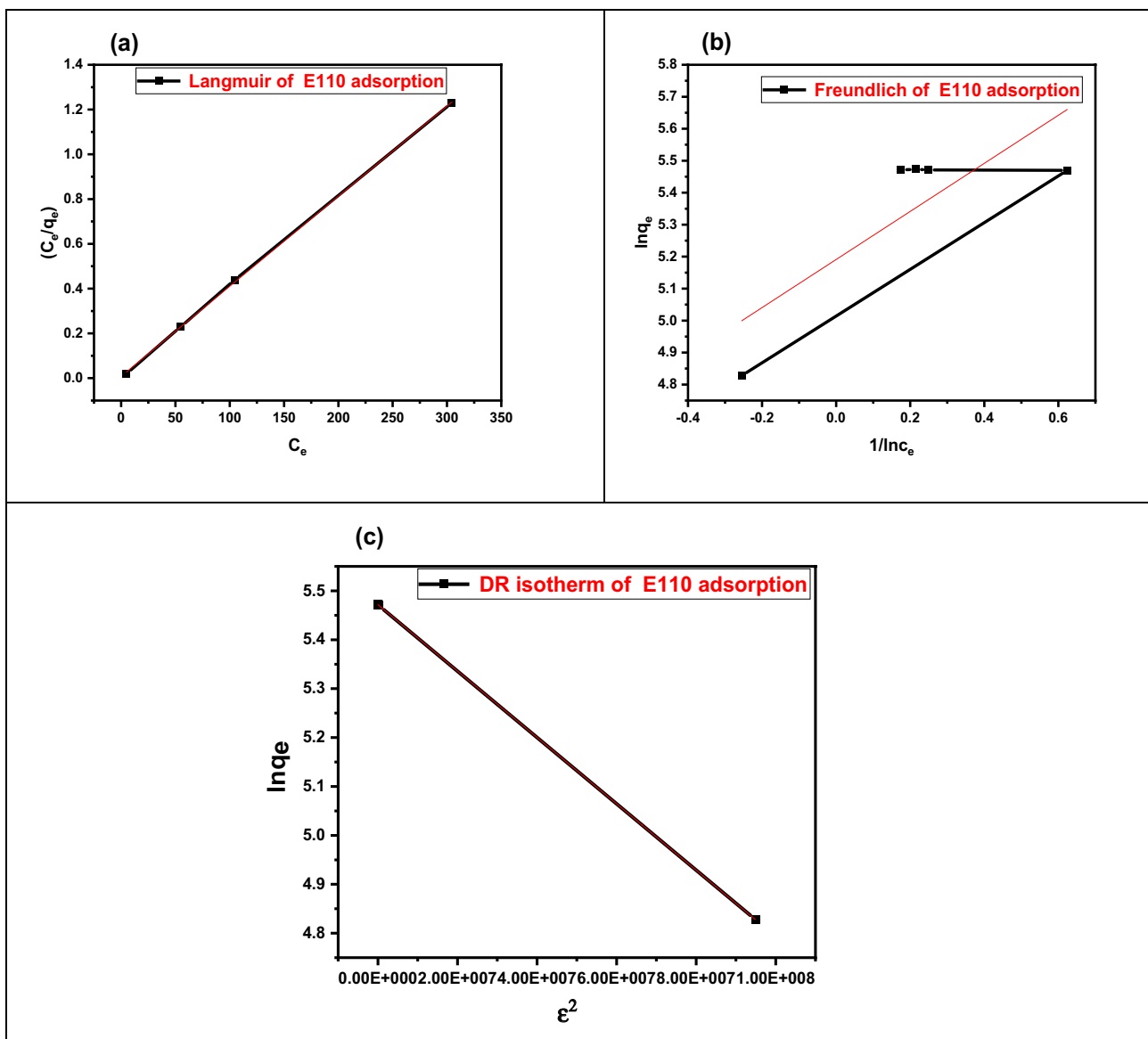
Fig. 11 Isotherm models of adsorption of E110 **a** Langmuir isotherm, **b** Freundlich isotherm, **c** DR isotherm

E110 adsorption increased from 185 mg/g to 237.6 mg/g, the capacity of the E122 adsorption increased from 187.2 mg/g to 249.5 mg/g, and the capacity of the E124 adsorption increased from 242 mg/g to 343 mg/g. With increasing the dose above (0.01 g), it was noticed that the capacity decreased from 237.6 mg/g to 83.08 mg/g, from 249.5 mg/g to 73.42 mg/g, and from 343 mg/g to 122.6 mg/g for E110, E122, and E124 adsorption, respectively.

Effect of initial concentration

The initial concentration parameter on E110, E122, and E124 adsorption into Bt@CTAB surface was investigated in the range of (50–400) ppm of the investigated anionic dyes

(E110, E122, and E124), and the other conditions were kept constant. Figure 10 (a-c) represents the influence of initial concentrations of the investigated dyes on the adsorption efficiency. It was noticed that the adsorption capacity for E110 and E122 increased (from 124.95 mg/g to 237.6 mg/g) and (from 124.96 mg/g to 249.5 mg/g), respectively, with the initial concentration dye increasing from 50 to 100 ppm. Additionally, the adsorption capacity for E124 enhanced from 124.9 mg/g to 343 mg/g with (E124) initial concentration increasing from 50 to 150 ppm. At concentrations of more than 100 ppm of (E110 and E122) and 150 ppm of E124, the adsorption capacity remains constant. Therefore, it can be indicated that the Bt@CTAB adsorption reached

Table 3 Adsorption isotherm parameters of E110, E122, and E124 by Bt@CTAB

System	Langmuir isotherm constants			
	K_L (L/g)	q_m (mg/g)	R^2	R_L
Bt@CTAB-E110	0.5088	248.75	0.99979	0.019
Bt@CTAB-E122	0.759	255.75	0.99999	0.013
Bt@CTAB-E124	2.2	350.87	0.99999	3.02×10^{-3}

System	Freundlich isotherm constants		
	K_F	n	R^2
Bt@CTAB-E110	179.657	1.33	0.66567
Bt@CTAB-E122	220.85	4	0.09112
Bt@CTAB-E124	267.676	−492.6	0.00478

System	DR isotherm constants			
	K_{DR}	E (kJ/mole)	q_m (mg/g)	R^2
Bt@CTAB-E110	6.7847×10^{-9}	8.584	237.87	0.99999
Bt@CTAB-E122	6.52809×10^{-9}	8.751	258.65	0.972
Bt@CTAB-E124	4.25418×10^{-9}	10.492	319.507	0.89995

equilibrium at a concentration of 100 ppm for (E110 and E122) and 150 ppm for E124.

Isotherm studies

Langmuir and Freundlich, and Dubinin–Radushkevich's isothermal models were utilized to study the mechanism of adsorption of E110, E122, and E124 onto the Bt@CTAB adsorbent. The three models' equations are presented in Eqs. 4, 5, and 6 in the experimental section.

Figure 11 (a-c) represents Langmuir, Freundlich, and Dubinin–Radushkevich plots for E110, E122, and E124 adsorption, while Table 3 shows the parameters (q_m, K_L, R_L, n, K_F, k_{DR}) of the three investigated isothermal models. From these results, the Langmuir isothermal model is well-matched with the three investigated dyes adsorption as its constants are more related to the E110, E122, and E124 adsorption process with higher R^2 values. R^2 values for the Langmuir model are 0.99979, 0.99999, and 0.99999 for E110, E122, and E124 removal, respectively, while R^2 values for the Freundlich model are 0.66567, 0.09112, and 0.00478 for E110, E122, and E124 adsorption, respectively. So, the adsorption here was monolayer adsorption. Besides that, the estimated values of R_L are calculated and they are founded to be less than 1.00 indicating the suitability of Bt@CTAB to be utilized as an adsorbent material for the studied anionic species (Akl et al. 2022a, 2022b).

Oscillation time and Kinetics investigation

Contact time of E110, E122, and E124 with Bt@CTAB adsorbent is a very essential parameter. So, it was investigated at different shaking times by using 0.01 g as a dose of Bt@CTAB adsorbent in pH-adjusted solutions (pH 5) of 100 ppm of (E110 and E122) and 150 ppm of (E124), and at room temperature. Figure 12 represents the influence of contact time on E110, E122, and E124 anionic species adsorption (Fig. 12a), pseudo-1st order of the investigated anionic species adsorption (Fig. 12b, d, f), and pseudo-2nd order of adsorption (Fig. 12c, e, g). In the beginning, the adsorption is very fast as the efficiency at 15 min reached 82.07% for E110, 88.32% for E122, and 86.66% for E124. Then as time increased from 15 to 120 min, the removal efficiency increased from (82.07 to 95.04%) and (from 88.32 to 99.5%) for E110 and E122, respectively, while the E124 removal efficiency increased from 86.66 to 97.47% with shaking time increasing from 15 to 240 min. With increasing shaking time of more than 120 min for E110/E122 and more than 240 min for E124, the efficiency stays constant which means that the removal efficiency reached equilibrium at 120 min for (E110 and E122) and 240 min for E124.

The two kinetic models, the pseudo-1st-order and the pseudo-2nd-order models (that are presented in Eqs. (9) and (10), respectively), have been investigated for identifying the well-fitted model with E110, E122, and E124 adsorption.

Fig. 12 a Effect of time on E110, E122, and E124 adsorption on Bt@CTAB adsorbent, **b** pseudo-1st order for E110 adsorption, **c** pseudo-2nd order for E110 adsorption, **d** pseudo-1st order for E122 adsorption, **e** pseudo-2nd order for E122 adsorption, **f** pseudo-1st order for E124 adsorption, and **g** pseudo-2nd order for E124 adsorption
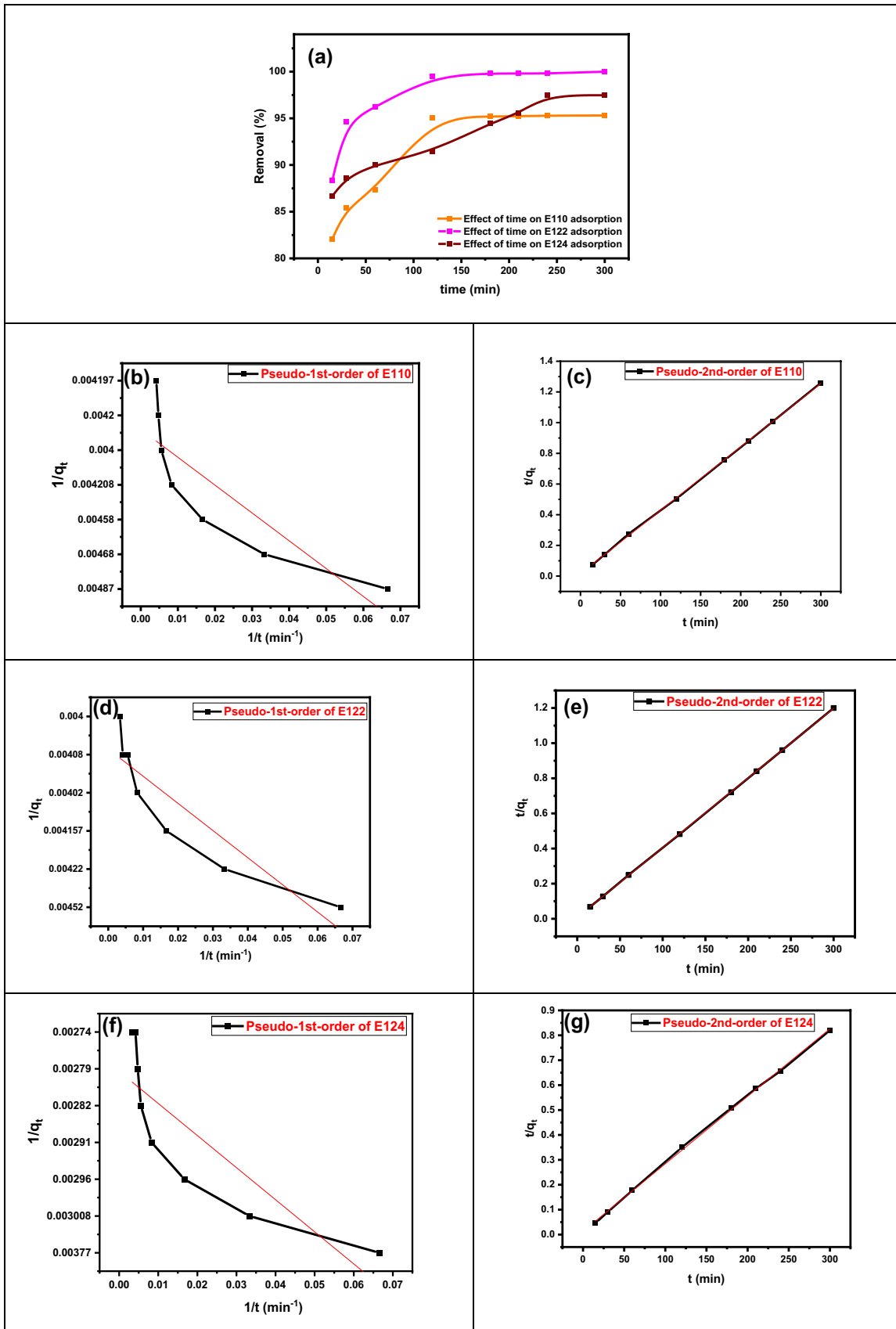
Table 4 represents the estimated 1st- and 2nd-order parameters (K_1, K_2, q_{e1}^{ads}, and q_{e2}^{ads}) and correlation coefficient R^2 values obtained from each investigated model nonlinear form. From these findings, investigated food dyes adsorption mechanism nature by the Bt@CTAB adsorbent can be illustrated. The calculated adsorption capacities in the case of pseudo-2nd order for E110, E122, and E124 were well-fitted with the experimental values. Besides, R^2 values of pseudo-1st order are very low 0.73122 for E110, 0.8045 for E122, and 0.726 for E124 in comparison with those of pseudo-2nd order 0.99982 for E110, 0.99998 for E122, and 0.99935 for E124. Therefore, pseudo-1st order cannot be used for explaining the adsorption nature here. So, E110, E122, and E124 adsorption onto Bt@CTAB adsorbent is well-fitted to pseudo-2nd order and the adsorption rate-limiting step is controlled by a chemical process (Ouachtak et al. 2021).

Effect of temperature and thermodynamics

The investigated free energy ($\Delta G°$), enthalpy ($\Delta H°$), and entropy ($\Delta S°$) thermodynamic parameters of the E110, E122, and E124 anionic dyes adsorption by Bt@CTAB adsorbent were obtained by examining anionic dyes adsorption in a temperature range of 298–318 K. Thermodynamic parameters and K_c, equilibrium constant were calculated as in Eqs. 11 and 12. Table 5 shows the estimated values of thermodynamic parameters, while Fig. S2 shows the plotted curves. As can be seen, the estimated negative $\Delta G°$ values prove that the E110, E122, and E124 adsorption on Bt@CTAB adsorbent is spontaneous in addition to the thermodynamic feasibility of the E110, E122, and E124 adsorption under the investigated temperature range. Also, negative charges of $\Delta H°$ estimate that the adsorption process was exothermic for E110, E122, and E124 adsorption. From $\Delta H°$ values that are higher than 80 kJ/mole, it was proven that the adsorption was chemisorption. Besides that, $\Delta S°$ charge (negative) reveals that E110/E122/E124 adsorption results in lower randomness and an increase in alignment. It was noticed that the decreasing E110, E122, and E124 adsorption with the temperature increases (Akl et al. 2022b).

Effect of ionic strength

As industrial wastewater has high concentrations of different solutes, so the ionic strength parameter considers an important parameter. It was investigated using different anions such as NaCl (0.1 M), Na_2CO_3 (0.1 M), CH_3COONa (0.1 M), and EDTA (0.1 M) at the optimum conditions of the investigated dyes adsorption. Figure S3 represents the influence of different anions on E110,

E122, and E124 adsorption on Bt@CTAB adsorbent. As shown in Fig. S3 for E110, E122, and E124 adsorption on the Bt@CTAB surface, the different anions at concentration 0.1 M do not significantly affect the investigated dyes adsorption.

Desorption and Regeneration

In order to Bt@CTAB reusability investigation, 5 cycles of E110, E122, and E124 adsorption–desorption were carried out at the optimum conditions. Several eluents were investigated and it was found that ethanol is the best among them. Figure 13a represents the effect of different eluents on the E110, E122, and E124 desorption, while Fig. 13b shows the obtained data of the repeated five cycles of E110, E122, and E124 adsorption–desorption using ethanol as eluent.

Removal of E110, E122, and E124 in Binary system

The maximum absorbances (λ_{max}) of the investigated dyes, E110 (486 nm), E122 (518 nm), and E124 (508 nm), are shown in Fig. 14. In addition, various binary systems were investigated such as E110-E122 (508 nm), E110-E124 (500 nm), E122-E124 (518 nm), and E110-E122-E124 (512 nm) which are present in Fig. 14. It was observed that after mixing the dyes together, new overlapped peaks were formed as presented in Fig. 14 (a-d). All the adsorption investigations were examined at each pollutant λ_{max}. As the organic pollutants (dyes) are present in real polluted water in multiple forms, so it is very essential to apply the Bt@CTAB clay material removal potential in the investigated dyes' binary systems. For the adsorption experiment, 0.01 g of Bt@CTAB was added to binary system solutions (50 ppm of each dye in the mixture) at pH 5. Then the mixture was shaken at 120 rpm at different time intervals. The equilibrium concentration of the adsorbates was calculated from UV–Vis data. The adsorption efficiency of anionic adsorbates is calculated using Eq. 2. Figure 15 represents the binary systems UV after adsorption by Bt@CTAB material. The adsorption reached its equilibrium after 3 h for E110-E122, E122-E124, and E110-E122-E124 binary systems that are present in Fig. 15a, c, d, respectively, while E110-E124 (Fig. 15b) reached equilibrium after 2 h.

Optimization through column investigations

The removal of (E110, E122, and E124) anionic food dyes by Bt@CTAB was investigated by applying column tests at optimum pH and temperature conditions (obtained from batch experiments). The utilization of Bt@CTAB adsorbent

Table 4 Kinetic parameters for the adsorption of E110, E122, and E124 by Bt@CTAB

System	Pseudo-1st-order model		
	K_1 (min^{-1})	q_{e1ads} (mg/g)	R^2
Bt@CTAB-E110	−14.3	0.178	0.73122
Bt@CTAB-E122	−13.84	0.194	0.8045
Bt@CTAB-E124	−14.7	0.168	0.726
System	Pseudo-2nd-order model		
	k_2 (g/(mg min))	q_{e2ads} (mg/g)	R^2
Bt@CTAB-E110	1.1076×10^{-3}	242.13	0.99982
Bt@CTAB-E122	1.924×10^{-3}	251.89	0.99998
Bt@CTAB-E124	5.55×10^{-4}	369	0.99935

Table 5 Thermodynamic parameters for the adsorption of E110, E122, and E124 onto Bt@CTAB

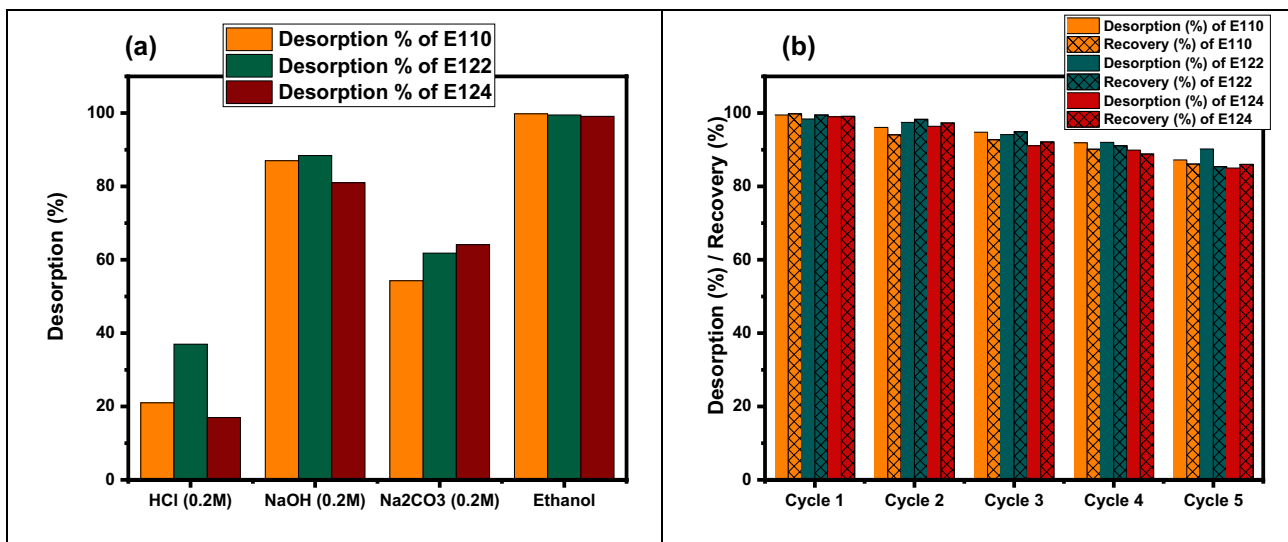| System	T (k)	K_c	$\Delta G°_{ads}$(KJ/mol)	$\Delta H°_{ads}$ (KJ/mol)	$\Delta S°_{ads}$ (J/mol K)
Bt@CTAB-E110	298	47.9	−9.56	−80	−236.6
	308	16.44	−7.167		
	318	6.296	−4.865		
Bt@CTAB-E122	298	1247.5	−17.66	−178.26	−540.7
	308	79.38	−11.21		
	318	14.05	−6.979		
Bt@CTAB-E124	298	26.7	−8.126	−82.08	−247.98
	308	11.02	−6.146		
	318	3.3	−3.173		

Fig. 13 a Desorption of E110, E122, and E124 from Bt@CTAB adsorbent by different eluents. **b** Repeated 5 cycles of E110, E122, and E124 adsorption–desorption with using ethanol as an eluent
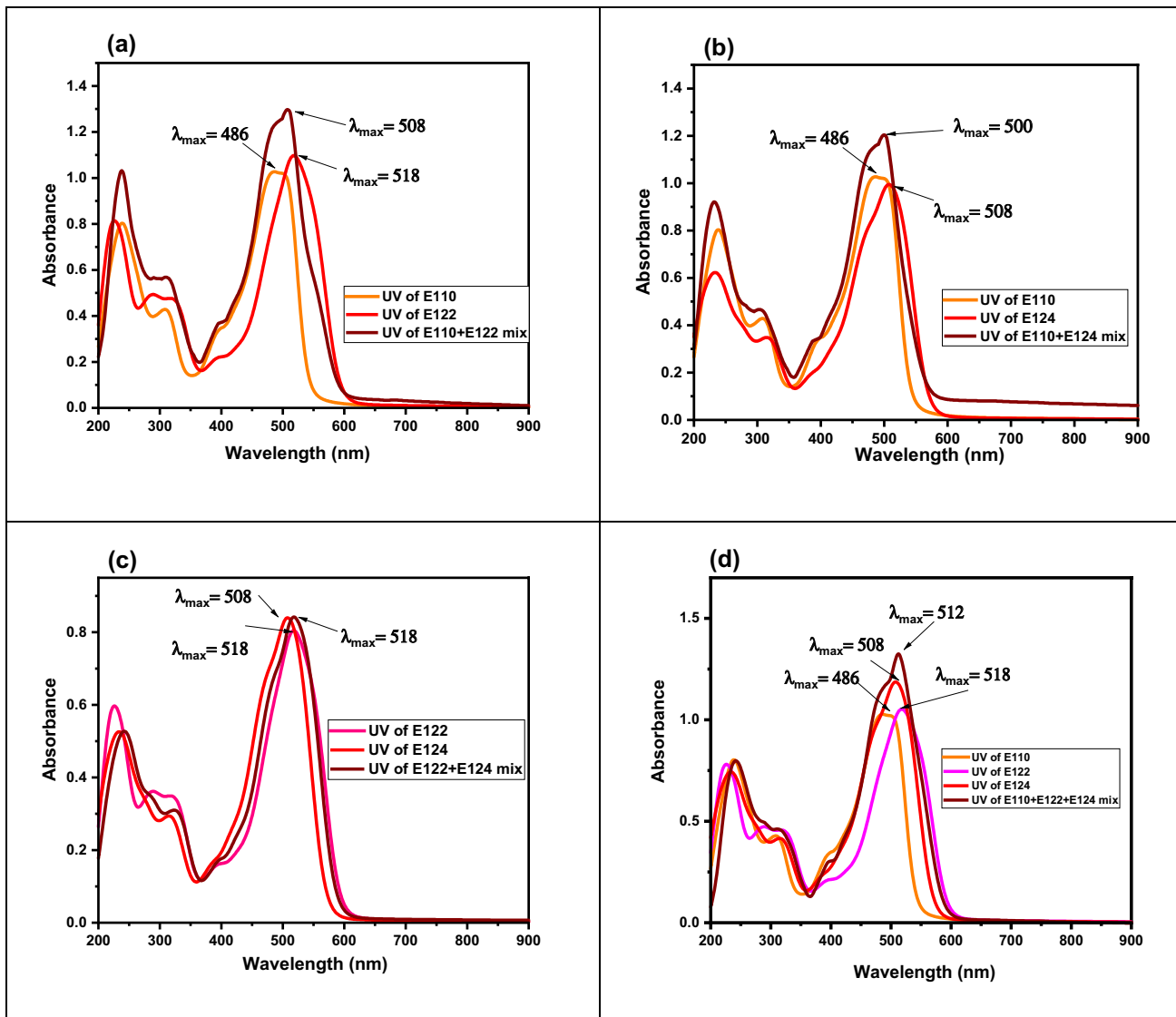
Fig. 14 UV data of **a** E110-E122 mix are compared with E110 and E122, **b** E110-E124 mix is compared with E110 and E124, **c** E122-E124 mix is compared with E122 and E124, and **d** E110-E122-E124 mix is compared with E110, E122, and E124

as a filter was examined, and the findings in Table 6 showed that E110, E122, and E124 dyes were removed with a percent higher than 98.5% using 0.01 g of the Bt@CTAB adsorbent, a column with a diameter 0.7 cm at a slow flow rate for the three investigated dyes. The maximum capacity for E124 was higher than that of E110 and E122.

Applications

Analysis of dyes in real water samples

The optimized experimental conditions were applied to real samples to evaluate the efficiency of Bt@CTAB for the adsorption of anionic dyes. By utilizing standard solutions, the calibration curves were obtained. The standard solutions (1.0 L) were prepared under the experimental conditions optimized above. The real investigated samples were tap water in our laboratory at Mansoura University and seawater in Damietta City. The obtained results are presented in Table 7. All spiked dyes were not naturally present in all of the samples. The recoveries were determined in the samples in which given amounts of each dye were spiked. The recoveries obtained were in the range of 98.33–99.87%. These findings indicate that Bt@CTAB adsorbent could be successfully applied to the determination of anionic dyes in real water.
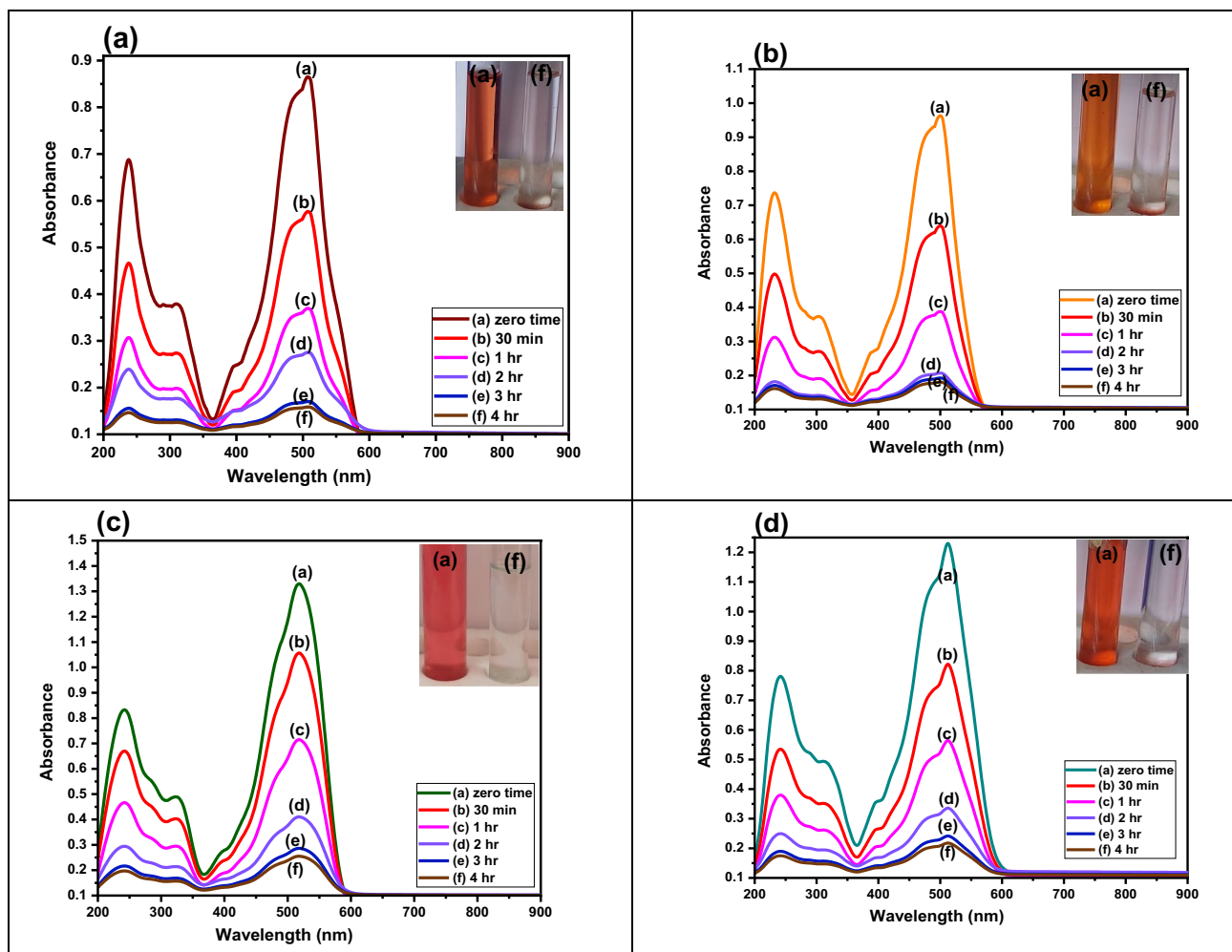
Fig. 15 UV data of **a** E110-E122 mix, **b** E110-E122 mix, **c** E122-E124 mix, and **d** E110-E122-E124 mix after adsorption by Bt@CTAB at different time intervals

Analysis of dyes in colored soft drinks and industrial food samples

The optimized experimental conditions of the E110 and E122 adsorption were applied to various samples that contain (E110 and E122) to evaluate the Bt@CTAB efficiency for anionic dyes sorption. The calibration curves were prepared with the standard solutions. The food samples were degassed carbonized drinks, candy, and jelly. Figure S4 illustrates that the E110 and E122 recovery from the examined samples was achieved with a percentage of higher than 99%. These results indicate that the Bt@CTAB material could be successfully applied to the recovery of anionic dyes from different samples.

Plausible mechanism of adsorption of E110, E122, and E122 onto Bt@CTAB

The plausible mechanism of adsorption of anionic species onto Bt@CTAB can be discussed according to the findings of optical images of Bt@CTAB and the Bt@CTAB loaded dyes and the FTIR studies as it is represented in the following section. Adsorbate–adsorbent interaction mechanism through the adsorption process generally occurred through electrostatic interactions, ion-exchanging, hydrogen bonds, etc. (Amosa et al. 2016; Kamat 1993). FTIR spectra after E110, E122, and E124 anionic species adsorption on the (Bt@CTAB) adsorbent surface are highly efficient in the adsorption mechanism illustration. Significant changes

Table 6 Column studies for the removal of the E110. E122, and E124 anionic dyes

Dose effect					
Dye	Fiber (gram)	Flow rate (ml/min)	Column diameter(cm)	Removal (%)	Adsorption capacity (mg/g)
E110	0.0025	0.42	0.7	21	210
	0.005			43.21	216.05
	0.01			96	240
	0.015			98.3	163.83
	0.02			99.1	123.875
	0.05			99.9	49.95
E122	0.0025	0.42	0.7	12.35	123.5
	0.005			47.11	235.55
	0.01			99.4	248.5
	0.015			99.9	166.5
	0.02			99.85	124.8125
	0.05			99.93	49.965
E124	0.0025	0.42	0.7	17.83	267.45
	0.005			41.03	307.725
	0.01			92	345
	0.015			93.14	232.85
	0.02			95.8	155.675
	0.05			97	72.75
Diameter effect					
E110	0.01	0.42	0.7	96	240
			0.9	89.3	223.25
E122	0.01	0.42	0.7	99.4	248.5
			0.9	91.1	227.75
E124	0.01	0.42	0.7	92	345
			0.9	84.45	316.69
Flow rate effect					
E110	0.01	0.42	0.7	96	240
		0.16			
E122	0.01	0.42	0.7	99.4	248.5
		0.16		99.97	249.925
E124	0.01	0.42	0.7	92	345
		0.16		98.9	370.875

were shown when the FTIR spectra of Bt@CTAB before investigated food dyes adsorption (Fig. 16 A.1) compared to those after adsorption [Fig. 16 (A.2), (A.3), and (A.4)]. The newly appeared peak at 1370 cm^{-1} in Bt@CTAB-E110, Bt@CTAB-E122, and Bt@CTAB-E124 spectra is related to the sulfonate stretching vibrational peak of the three dyes (Liu et al. 2018). Also, new peaks appeared that correspond to aromatic alkene C=C appeared at 1525 cm^{-1} for the Bt-CTAB material after the adsorption of the three dyes (Liu et al. 2018; Ziane et al. 2018). The peak at 3452 cm^{-1} became broader after E110, E122, and E124 adsorption which may be attributed to hydrogen bond formation. These new peaks are great evidence for E110, E122, and E124 adsorption on the Bt@CTAB surface. CTAB characteristic bands still present with slight shifts after adsorption which confirm that CTAB does not leach into the solution during adsorption batch experiments. The aim of the modification here is to change the clay surface charge from -ve to +ve and to increase surface hydrophobicity. So, there are two expected interactions between investigated dyes (E110, E122, and E124) and Bt@CTAB material are

1. Electrostatic interaction between the SO$_3^-$ negative charge of E110, E122, and E124 and the positive charge of CTAB (-N$^+$(CH$_3$)$_3$) head.

2. The hydrogen bonding between the OH group of Bt@CTAB material and the hydrogen group of (C$_6$H$_6$) ring in the three investigated food dyes.

Table 7 Analytical results of adsorption of E110, E122, and E124 anionic dyes in real water samples utilizing Bt@CTAB adsorbent (n = 5)

Sample	Dye	Spiked (µg. mL^{-1})	Measured (µg. mL^{-1})	Recovered (µg. mL^{-1})	Recovery (%)
Tap water	E110	0.00	0.00	0.00	0.00
		50	0.1	49.9	99.89
		100	5.08	94.92	99.87
	E122	0.00	0.00	0.00	0.00
		50	0.84	49.16	98.34
		100	1.3	98.95	99.14
	E124	0.00	0.00	0.00	0.00
		100	1.2	98.8	99.82
		150	13.81	136.19	99.27
Sea water	E110	0.00	0.00	0.00	0.00
		50	0.32	49.68	99.39
		100	6	94	98.8
	E122	0.00	0.00	0.00	0.00
		50	0.75	49.25	98.53
		100	1	99	99.19
	E124	0.00	0.00	0.00	0.00
		100	1.7	98.3	99.32
		150	14.5	135.5	98.76
Sea water	E110	0.00	0.00	0.00	0.00
		50	0.21	49.79	99.61
		100	5.5	94.5	99.34
	E122	0.00	0.00	0.00	0.00
		50	0.73	49.27	99.47
		100	1.3	98.7	98.57
	E124	0.00	0.00	0.00	0.00
		100	2.1	97.9	98.91
		150	15.1	134.9	98.33

In Fig. 16B, schematic illustration of E110, E122, and E124 anionic species' adsorption on the Bt@CTAB adsorbent surface is presented as an example of the investigated anionic species adsorption mechanism in this study.

Performance of Bt@CTAB

The Bt@CTAB material provides the capability for E110, E122, and E124 anionic species separation and removal from several water samples achieved with high efficiency. Table 8 represents a comparison between the Bt@CTAB performances with other cited adsorbents. It was observed that Bt@CTAB material when comparing different adsorbents for remediation of E110, E122, and E124, the sorption capacity and the type of adsorbent, adsorbent dose, initial concentration, and equilibrium time on which the sorption is performed should be taken into consideration. Finally, the Bt@CTAB has high capacities and efficiencies for the E110, E122, and E124 recovery compared to other mentioned adsorbents are found in Table 8.

Conclusion

In order to find low-cost adsorbents having pollutant-binding capacities is highly significant for efficient water treatment.

The results of the present study reveal that:

a. Bt@CTAB organoclay may be a highly applicable adsorbent for the removal of E110, E122, and E124 anionic food dyes from aqueous solutions.
b. Modification of Bt by CTAB significantly increased the nitrogen-containing groups on the surface of Bt@CTAB organoclay with a remarkable change in textural properties and surface morphology.
c. The adsorption of E110, E122, and E124 anionic food dyes was dependent on initial concentration, reaction temperature, and pH.
d. The equilibrium of the adsorption process could is well described by Langmuir adsorption isotherms, i.e., monolayer adsorption on a homogenous surface. The kinetic studies follow a pseudo-2nd-order kinetic model.
e. The negative values of ($\Delta G°$) and ($\Delta H°$) thermodynamic parameters clarify the spontaneous and exothermic nature of the adsorption technique.
f. In this study, the prepared Bt@CTAB adsorbent has high removal efficiency of anionic food dyes at optimum batch sorption conditions with maximum sorption capacity of 238 mg/g, 248.75 mg/g, and 358.25 mg/g, respectively, mg.g^{-1} for E110, E122, and E124, respectively, that was achieved within 120–240 min.
g. The as-prepared surfactant-supported organoclay composite (BT@CTAB) was applied for the removal of E110, E122, and E124 food dyes in batch and column modes.
h. The as-prepared surfactant-supported organoclay composite (BT@CTAB) was applied for the removal of E110, E122, and E124 food dyes in single and multi-component dye solution modes

Fig. 16 (**A**) FTIR spectra of (a) BT@CTAB, (b) Bt@CTAB-E110, (c) Bt@CTAB-E122, and (d) Bt@CTAB-E124; (**B**) schematic illustration of anionic species' adsorption on the Bt@CTAB adsorbent surface
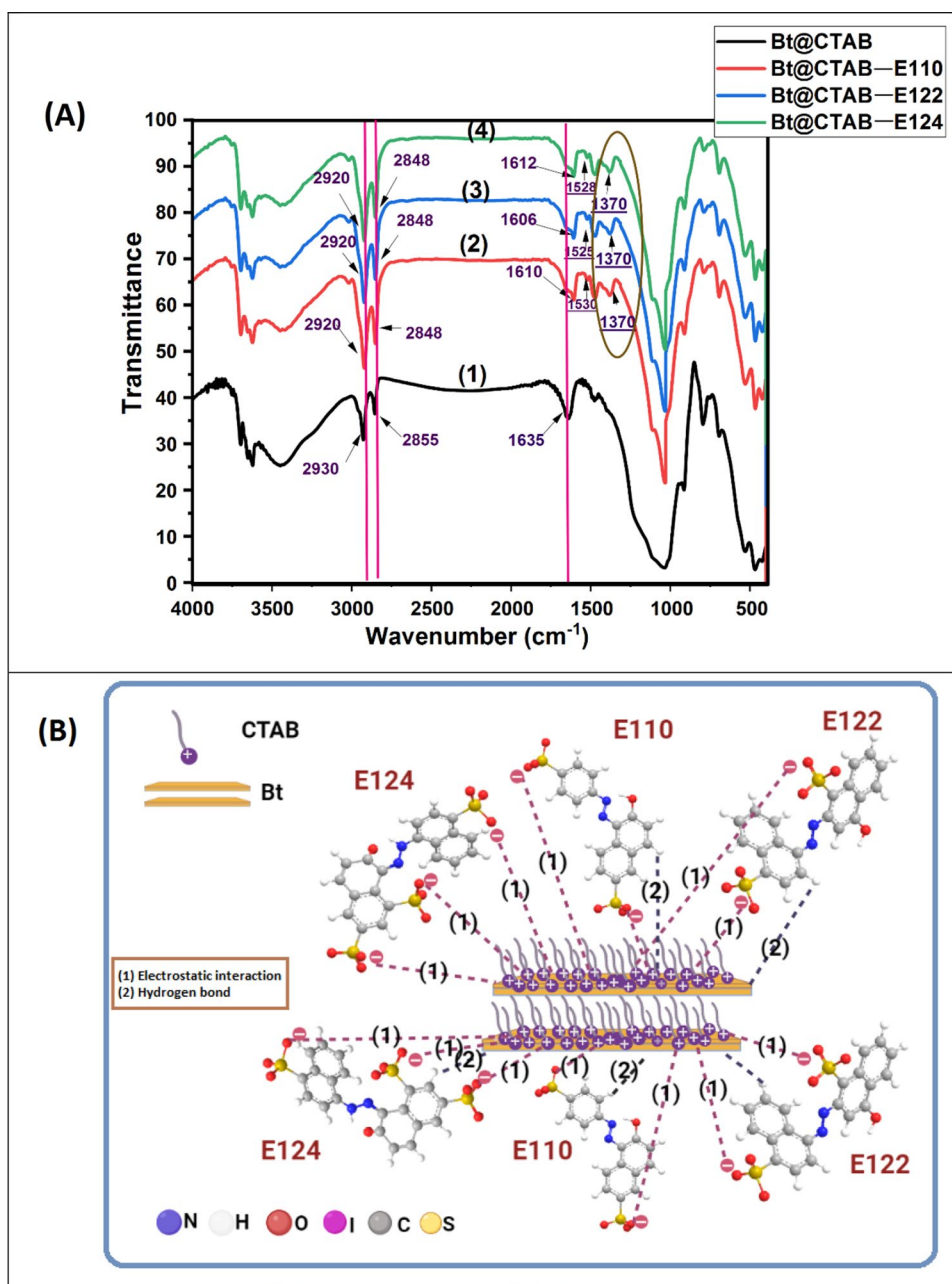
i. The removal of E110, E122, and E124 from natural water and industrial food samples was successfully applied using Bt@CTAB.
j. Submersion of the Bt@CTAB-loaded dyes samples in 5 ml of ethanol resulted in the desorption of more than 90% of the adsorbed dyes.
k. The uptake of E110, E122, and E124 using such Bt@CTAB is highly comparable to the previous commercial adsorbents used for the removal of E110, E122, and E124.
l. The adsorption mechanism was proposed to be due to electrostatic interaction (between N^+ of semicarbazide moiety and dyes SO_3 group) and the formation of the hydrogen bond.
m. In conclusion, the present work well demonstrated the potential of this technique for environmental remediation.

Table 8 Comparison of adsorption capacity of E110, E122, and E124 onto Bt@CTAB with previously reported studies

Adsorbate	Adsorbent	Adsorbent dose	Initial concentration	Equilibrium time	Sorption capacity (mg/g)	References
E110	Mesoporous carbon	0.2 g/L	50 ppm	240 min	204.1	Ahmad et al. (2019)
	Activated carbon	1 g/L	300 ppm	240 min	199.7	Lopes et al. (2021)
	Fe_3O_4–OT bioadsorbent	0.02 g/L	16 ppm	20 min	53.59	Sadegh et al. (2022)
	Cassava sievate biomass	0.1 g	150 ppm	90 min	0.091	Chukwuemeka-Okorie et al. (2021)
	Bt@CTAB	0.01 g/25 ml	100 ppm	120 min	238	Present study
E122	$0.1SnO_2$–$0.9CeO_2$	1 g/L	20 ppm	20 min	22.10	Ali et al. (2022)
	$0.15SnO_2$–$0.85CeO_2$				22.88	
	$0.2SnO_2$–$0.8CeO_2$				21.16	
	$0.3SnO_2$–$0.7CeO_2$				18.33	
	natural diatomite (ND)	1 g/L	50 ppm	30 min	12 mg/g	Labiod et al. (2022)
	Ni/Zn-layered double hydroxide (Ni/Zn LDH)	30 mg/L	50 ppm	60 min	223 mg/g	Nait-Merzoug et al. (2021)
	Bt@CTAB	0.01 g/25 ml	100 ppm	120 min	248.75	Present study
E124	Fe_3O_4@SiO_2-CMK-8, MNCs	0.1 g	50 ppm	20 min	78.74	Toutounchi et al. (2021)
	NH_2-MMNC	80 mg	50 ppm	30 min	58.8	Sojoudi et al. (2016)
	polyamidoamine–cyclodextrin crosslinked copolymer (PAMAM-CD)	50 mg	340 ppm	90 min	254.3	Li and Lei (2012)
	Bt@CTAB	0.01 g/25 ml	150 ppm	240 min	358.25	Present study

Declarations

Competing interests The authors declare that they have no competing interests.

Ethical approval Not applicable to this study.

Consent for publication Not applicable to this study.

Consent to participate Not applicable to this study.

References

Abd-Ellatif WR, Mahmoud NG, Hashem AA, El-Aiashy MK, Ezzo EM, Mahmoud SA (2022) Efficient photodegradation of E124 dye using two-dimensional Zn-Co LDH: kinetic and thermodynamic studies. Environ Technol Innov 2022:27

Affat SS (2021) Classifications, advantages, disadvantages, toxicity effects of natural and synthetic dyes: a review. Univ Thi-Qar J Sci 8:130–135

Ahmad ZU, Yao L, Wang J, Gang DD, Islam F, Lian Q et al (2019) Neodymium embedded ordered mesoporous carbon (OMC) for enhanced adsorption of sunset yellow: characterizations, adsorption study and adsorption mechanism. Chem Eng J 359:814–826

Akl MA, Hashem MA, Ismail MA, Abdelgalil DA (2022a) Novel diaminoguanidine functionalized cellulose: synthesis, characterization, adsorption characteristics and application for ICP-AES

determination of copper(II), mercury(II), lead(II) and cadmium(II) from aqueous solutions. BMC Chem 2022:16

Akl MA, Hashem MA, Mostafa AG (2022b) Synthesis, characterization, antimicrobial and photocatalytic properties of nano-silver-doped flax fibers. Polym Bull. https://doi.org/10.1007/s00289-022-04531-5

Alexander JA, Ahmad Zaini MA, Surajudeen A, Aliyu ENU, Omeiza AU (2019) Surface modification of low-cost bentonite adsorbents—a review. Particul Sci Technol 37:534–545

Alham A, Ibraimov A, Alimzhanova M, Mamedova M (2022) Natural material shungite as solid-phase extraction sorbent for the extraction of red synthetic dye Ponceau 4R from tap water, wine, and juice. Food Anal Methods 15:707–716

Ali I, Kon'kova T, Liberman E, Simakina E, ALOthman ZA, Alomar TS et al (2022) Preparation and characterization of SnO2-CeO2 nanocomposites: sorption, modeling and kinetics for azorubine dye removal in water. J Mol Liq 2022:346

Amosa MK, Jami MS, Alkhatib MFR (2016) Electrostatic biosorption of COD, Mn and H2S on EFB-based activated carbon produced through steam pyrolysis: an analysis based on surface chemistry, equilibria and kinetics. Waste Biomass Valorization 7:109–124

Ashraf RS, Abid Z, Shahid M, Rehman ZU, Muhammad G, Altaf M et al (2021) Methods for the treatment of wastewaters containing dyes and pigments

Avila MC, Lick ID, Comelli NA, Ruiz ML (2021) Adsorption of an anionic dye from aqueous solution on a treated clay. Groundw Sustain Dev 2021:15

Bahrudin NN, Nawi MA, Jawad AH, Sabar S (2020) Adsorption characteristics and mechanistic study of immobilized chitosan-montmorillonite composite for methyl orange removal. J Polym Environ 28:1901–1913

Balayeva OO, Azizov AA, Muradov MB, Alosmanov RM (2021) Removal of tartrazine, ponceau 4R and patent blue V hazardous food dyes from aqueous solutions with ZnAl-LDH/PVA nanocomposite. J Dispers Sci Technol 44:1133–1146

Berradi M, Hsissou R, Khudhair M, Assouag M, Cherkaoui O, El Bachiri A et al (2019) Textile finishing dyes and their impact on aquatic environs. Heliyon 2019:5

Chukwuemeka-Okorie HO, Ekuma FK, Akpomie KG, Nnaji JC, Okereafor AG (2021) Adsorption of tartrazine and sunset yellow anionic dyes onto activated carbon derived from cassava sievate biomass. Appl Water Sci 2021:11

el Haouti R, Ouachtak H, el Guerdaoui A, Amedlous A, Amaterz E, Haounati R et al (2019) Cationic dyes adsorption by Na-Montmorillonite Nano Clay: experimental study combined with a theoretical investigation using DFT-based descriptors and molecular dynamics simulations. J Mol Liq 2019:290

El Ouardi M, Laabd M, Oualid HA, Brahmi Y, Abaamrane A (2019) Efficient removal of p-nitrophenol from water using montmorillonite clay: insights into the adsorption mechanism, process optimization, and regeneration. Environ Sci Pollut Res 2019:19615–19631

El-Kowrany SI, El-Zamarany EA, El-Nouby KA, El-Mehy DA, Abo Ali EA, Othman AA et al (2016) Water pollution in the Middle Nile Delta, Egypt: an environmental study. J Adv Res 7:781–794

Gamoudi S, Srasra E (2019) Adsorption of organic dyes by HDPy+-modified clay: effect of molecular structure on the adsorption. J Mol Struct 1193:522–531

Hamada MS, Jabal RA (2022) Doped (Ag) ZnO nanoparticles for removal of azo dyes from aqueous solutions. IJCBS. www.iscientific.org/Journal.html

Haounati R, Ouachtak H, el Haouti R, Akhouairi S, Largo F, Akbal F et al (2021) Elaboration and properties of a new SDS/CTAB@Montmorillonite organoclay composite as a superb adsorbent for the removal of malachite green from aqueous solutions. Sep Purif Technol 2021:255

Huang Z, Li Y, Chen W, Shi J, Zhang N, Wang X et al (2017) Modified bentonite adsorption of organic pollutants of dye wastewater. Mater Chem Phys 202:266–276

Hube S, Eska M, Hrafnkelsdóttir KF, Bjarnadóttir B, Bjarnadóttir MÁ, Axelsdóttir S et al (2020) Direct membrane filtration for wastewater treatment and resource recovery: a review. Sci Total Environ 2020:710

Husien S, El-taweel RM, Salim AI, Fahim IS, Said LA, Radwan AG (2022) Review of activated carbon adsorbent material for textile dyes removal: preparation, and modelling. Curr Res Green Sustain Chem 2022:100325

Iwuozor KO, Ighalo JO, Emenike EC, Ogunfowora LA, Igwegbe CA (2021) Adsorption of methyl orange: a review on adsorbent performance. Curr Res Green Sustain Chem 4:100179

Kamat PV (1993) Photochemistry on nonreactive and reactive (semiconductor) surfaces. Chem Rev 93:267–300

Karri RR, Ravindran G, Dehghani MH (2021) Wastewater—sources, toxicity, and their consequences to human health. In: Soft computing techniques in solid waste and wastewater management. Elsevier, pp 3–33

Labiod K, Hazourli S, Bendaia M, Tlili M, Aitbara A, Graine R et al (2022) Removal of azo dye carmoisine by adsorption process on diatomite. Adsorpt Sci Technol 2022:1–17

Laptev AY, Rozhmanova NB, Tikhomirova TI, Lanin SN, Nesterenko PN (2021) Adsorption of synthetic dyes under the conditions of capillary zone electrophoresis. Moscow Univ Chem Bull 76:127–132

Largo F, Haounati R, Akhouairi S, Ouachtak H, el Haouti R, el Guerdaoui A et al (2020) Adsorptive removal of both cationic and anionic dyes by using sepiolite clay mineral as adsorbent: experimental and molecular dynamic simulation studies. J Mol Liq 2020:318

Leulescu M, Rotaru A, Moanţă A, Iacobescu G, Pălărie I, Cioateră N et al (2021) Azorubine: physical, thermal and bioactive properties of the widely employed food, pharmaceutical and cosmetic red azo dye material. J Therm Anal Calorim 143:3945–3967

Li N, Lei XM (2012) Adsorption of ponceau 4R from aqueous solutions by polyamidoamine-cyclodextrin crosslinked copolymer. J Incl Phenom Macrocycl Chem 74:167–176

Lima VVC, Dalla Nora FB, Peres EC, Reis GS, Lima ÉC, Oliveira MLS et al (2019) Synthesis and characterization of biopolymers functionalized with APTES (3-aminopropyltriethoxysilane) for the adsorption of sunset yellow dye. J Environ Chem Eng 2019:7

Liu J, Zhao C, Tu H, Yang J, Li F, Li D et al (2017) U(VI) adsorption onto cetyltrimethylammonium bromide modified bentonite in the presence of U(VI)-CO3 complexes. Appl Clay Sci 135:64–74

Liu A, Wang CC, Wang C, Fu H, Peng W, Cao YL et al (2018) Selective adsorption activities toward organic dyes and antibacterial performance of silver-based coordination polymers. J Colloid Interface Sci 512:730–739

Lopes GKP, Zanella HG, Spessato L, Ronix A, Viero P, Fonseca JM et al (2021) Steam-activated carbon from malt bagasse: optimization of preparation conditions and adsorption studies of sunset yellow food dye. Arab J Chem 2021:14

Mallkpour S, Behranvand V (2021) Polyurethane sponge modified by alginate and activated carbon with abilities of oil absorption, and selective cationic and anionic dyes clean-up. J Clean Prod 2021:312

Micheletti L, Coldibeli B, Salamanca-Neto CAR, Almeida LC, Sartori ER (2020) Assessment of the use of boron-doped diamond electrode for highly sensitive voltammetric determination of the azo-dye carmoisine E−122 in food and environmental matrices. Talanta 2020:220

Mishra AK, Allauddin S, Narayan R, Aminabhavi TM, Raju KVSN (2012) Characterization of surface-modified montmorillonite nanocomposites. Ceram Int 38:929–934

Monteiro MKS, de Oliveira VRL, dos Santos FKG, de Barros Neto EL, de Lima Leite RH, Aroucha EMM et al (2018) Influence of the ionic and nonionic surfactants mixture in the structure and properties of the modified bentonite clay. J Mol Liq 272:990–998

Moore L (1999) Textiles and clothing. Britain's trade and economic structure

Moslemizadeh A, Khezerloo-ye Aghdam S, Shahbazi K, Khezerloo-ye Aghdam H, Alboghobeish F (2016) Assessment of swelling inhibitive effect of CTAB adsorption on montmorillonite in aqueous phase. Appl Clay Sci 127–128:111–122

Mostafa AG, El-Mekbaty A, Hashem MA, Akl MA (2021) Selective separation of Cu(II) from a single metal Ion solution by using O-amino thiophenol-modified flax fiber. Egypt J Chem 64:1701–1708

Motawie AM, Madany MM, El-Dakrory AZ, Osman HM, Ismail EA, Badr MM et al (2014) Physico-chemical characteristics of nano-organo bentonite prepared using different organo-modifiers. Egypt J Pet 23:331–338

Muhammad N, Nafees M, Ge L, Khan MH, Bilal M, Chan WP et al (2021) Assessment of industrial wastewater for potentially toxic elements, human health (dermal) risks, and pollution sources: a case study of Gadoon Amazai industrial estate, Swabi, Pakistan. J Hazard Mater 419:126450

Nait-Merzoug A, Guellati O, Djaber S, Habib N, Harat A, El-Haskouri J et al (2021) Ni/Zn layered double hydroxide (LDH) micro/nanosystems and their azorubine adsorption performance. Appl Sci 11:8899

Ouachtak H, Akhouairi S, Ait Addi A, Ait Akbour R, Jada A, Douch J et al (2018) Mobility and retention of phenolic acids through a goethite-coated quartz sand column. Colloids Surf A Physicochem Eng Asp 546:9–19

Ouachtak H, el Guerdaoui A, Haounati R, Akhouairi S, el Haouti R, Hafid N et al (2021) Highly efficient and fast batch adsorption of orange G dye from polluted water using superb organo-montmorillonite: experimental study and molecular dynamics investigation. J Mol Liq 2021:335

Prusty S, Pradhan S, Mishra S (2021) Ionic liquid as an emerging alternative for the separation and recovery of Nd, Sm and Eu using solvent extraction technique—a review. Sustain Chem Pharm 21:100434

Rafaqat S, Ali N, Torres C, Rittmann B (2022) Recent progress in treatment of dyes wastewater using microbial-electro-Fenton technology. RSC Adv 12:17104–17137

Rizzi V, Gubitosa J, Fini P, Romita R, Agostiano A, Nuzzo S et al (2020) Commercial bentonite clay as low-cost and recyclable "natural" adsorbent for the Carbendazim removal/recover from water: overview on the adsorption process and preliminary photodegradation considerations. Colloids Surf A Physicochem Eng Asp 2020:602

Sadegh N, Haddadi H, Asfaram A (2022) Synthesis of a green magnetic biopolymer derived from oak fruit hull tannin for the efficient and simultaneous adsorption of a mixture of Malachite Green and Sunset Yellow dyes from aqueous solutions. New J Chem 46:11862–11876

Salah BA, Gaber MS, Kandil AHT (2019) The removal of uranium and thorium from their aqueous solutions by 8-hydroxyquinoline immobilized bentonite. Minerals 2019:9

Salahuddin NA, El-Daly HA, el Sharkawy RG, Nasr BT (2018) Synthesis and efficacy of PPy/CS/GO nanocomposites for adsorption of ponceau 4R dye. Polymer (guildf) 146:291–303

Saleem J, Bin SU, Hijab M, Mackey H, McKay G (2019) Production and applications of activated carbons as adsorbents from olive stones. Biomass Convers Biorefin 9:775–802

Saleh MO, Hashem MA, Akl MA (2021) Removal of Hg (II) metal ions from environmental water samples using chemically modified natural sawdust. Egypt J Chem 64:1027–1034

Shi S, Liang Y, Jiao N (2020) Electrochemical oxidation induced selective C–C bond cleavage. Chem Rev 121:485–505

Shirzad-Siboni M, Khataee A, Hassani A, Karaca S (2015) Preparation, characterization and application of a CTAB-modified nanoclay for the adsorption of an herbicide from aqueous solutions: kinetic and equilibrium studies. C R Chim 18:204–214

Sojoudi M, Shariati S, Khabazipour M (2016) Amine functionalized kit-6 mesoporous magnetite nanocomposite as an efficient adsorbent for removal of Ponceau 4R dye from aqueous solutions. Iran Chem Soc Anal Bioanal Chem Res 3:287–298

Solotchina EP, Sklyarov E, Solotchin PA, Vologina EG, Sklyarova OA (2014) Mineralogy and crystal chemistry of carbonates from the Holocene sediments of Lake Kiran (western Transbaikalia): connection with paleoclimate. www.elsevier.com/locate/rgg

Srivastav AL, Ranjan M (2020) Inorganic water pollutants. Inorg Pollut Water 2020:1–15

Tamjidi S, Moghadas BK, Esmaeili H, Shakerian Khoo F, Gholami G, Ghasemi M (2021) Improving the surface properties of adsorbents by surfactants and their role in the removal of toxic metals from wastewater: a review study. Process Saf Environ Protect 148:775–795

Tebeje A, Worku Z, Nkambule TTI, Fito J (2022) Adsorption of chemical oxygen demand from textile industrial wastewater through locally prepared bentonite adsorbent. Int J Environ Sci Technol 19:1893–1906

Toutounchi S, Shariati S, Mahanpoor K (2021) Application of magnetic ordered mesoporous carbon nanocomposite for the removal of Ponceau 4R using factorial experimental design. SILICON 13:1561–1573

Vaia RA, Teukolsky RK, Giannelis EP (1994) Interlayer structure and molecular environment of alkylammonium layered silicates. Chem Mater 6:1017–1022

Waghchaure RH, Adole VA, Jagdale BS (2022) Photocatalytic degradation of methylene blue, rhodamine B, methyl orange and Eriochrome black T dyes by modified ZnO nanocatalysts: a concise review. Inorg Chem Commun 2022:109764

Wang LW, Wang RZ, Oliveira RG (2009) A review on adsorption working pairs for refrigeration. Renew Sustain Energy Rev 13:518–534

Wang Y, Jiang Q, Cheng J, Pan Y, Yang G, Liu Y et al (2021) Synthesis and characterization of CTAB-modified bentonite composites for the removal of Cs+. J Radioanal Nucl Chem 329:451–461

WHO G (2017) Guidelines for drinking-water quality. World Health Organization 55:1023–1024

Yaghmaeiyan N, Mirzaei M, Delghavi R (2022) Results in Chemistry Montmorillonite clay: introduction and evaluation of its applications in different organic syntheses as catalyst: a review. Results Chem 4:100549

Youssef AMAM, Al-Awadhi MM (2013) Adsorption of acid dyes onto bentonite and surfactant-modified bentonite. J Anal Bioanal Tech 2013:4

Zamora-Ledezma C, Negrete-Bolagay D, Figueroa F, Zamora-Ledezma E, Ni M, Alexis F et al (2021) Heavy metal water pollution: a fresh look about hazards, novel and conventional remediation methods. Environ Technol Innov 22:101504

Zhu Y, Cui Y, Peng Y, Dai R, Chen H, Wang Y (2023) Preparation of CTAB intercalated bentonite for ultrafast adsorption of anionic

dyes and mechanism study. Colloids Surf A Physicochem Eng Asp 2023:658

Ziane S, Bessaha F, Marouf-Khelifa K, Khelifa A (2018) Single and binary adsorption of reactive black 5 and Congo red on modified dolomite: performance and mechanism. J Mol Liq 249:1245–1253

Zou W, Gao B, Sik Y, Dong L (2019) Chemosphere Integrated adsorption and photocatalytic degradation of volatile organic compounds (VOCs) using carbon-based nanocomposites: a critical review. Chemosphere 218:845–859